Carderock Division,
Naval Surface Warfare Center
Bethesda, Maryland 20084-5000

Carderock Div, NSWC/SHD-1395-01. October 1992

Ship Hydromechanics Department
Research and Development Report

COMPUTATIONAL FLUID DYNAMICS IN SUPPORT OF THE LARGE CAVITATION CHANNEL

BY

EUGENE H. GOTIMER
CHENG-WEN LIN
JAMES BLANTON

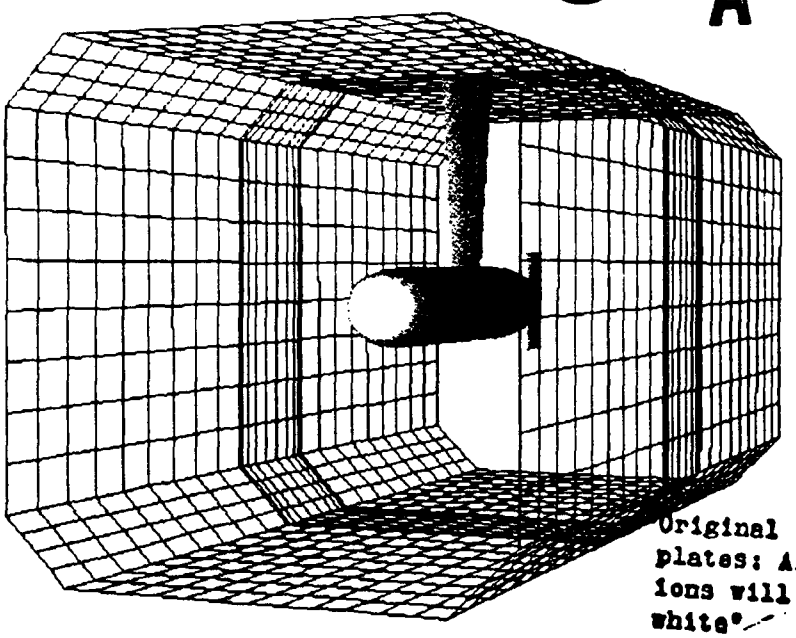

Original contains color plates: All DTIC reproductions will be in black and white.

APPROVED FOR PUBLIC RELEASE:
DISTRIBUTION UNLIMITED.

CDNSWC/SHD-1395-01 COMPUTATIONAL FLUID DYNAMICS IN SUPPORT OF THE LARGE CAVITATION CHANNEL

SECURITY CLASSIFICATION OF THIS PAGE

REPORT DOCUMENTATION PAGE

Form Approved OMB No. 0704-0188

1a. REPORT SECURITY CLASSIFICATION UNCLASSIFIED	1b. RESTRICTIVE MARKINGS
2a. SECURITY CLASSIFICATION AUTHORITY	3. DISTRIBUTION/AVAILABILITY OF REPORT
2b. DECLASSIFICATION/DOWNGRADING SCHEDULE	Approved for public release; distribution unlimited.
4. PERFORMING ORGANIZATION REPORT NUMBER(S) CARDEROCKDIV, NSWC/SHD-1395-01	
6a. NAME OF PERFORMING ORGANIZATION Carderock Division Naval Surface Warfare Center 6b. OFFICE SYMBOL (*if applicable*) Code 1521	7a. NAME OF MONITORING ORGANIZATION
6c. ADDRESS (*City, State and Zip Code*) Bethesda, MD 20084-5000	7b. ADDRESS (*City, State, and Zip Code*)
8a. NAME OF FUNDING/SPONSORING ORGANIZATION Carderock Division Naval Surface Warfare Center 8b. OFFICE SYMBOL (*if applicable*) Code 1502	9. PROCUREMENT INSTRUMENT IDENTIFICATION NUMBER
8c. ADDRESS (*City, State and Zip Code*) Bethesda, MD 20084-5000	10. SOURCE OF FUNDING NUMBERS PROGRAM ELEMENT NO. 65861N; PROJECT NO. WX2201; TASK NO.; WORK UNIT ACCESSION NO. DN#501172

11. TITLE (*Include Security Classification*)

COMPUTATIONAL FLUID DYNAMICS IN SUPPORT OF THE LARGE CAVITATION CHANNEL

12. PERSONAL AUTHOR(S) Eugene H. Gotimer, Cheng-Wen Lin, James Blanton

13a. TYPE OF REPORT	13b. TIME COVERED	14. DATE OF REPORT (*Year, Month, Day*)	15. PAGE COUNT
Final	FROM Aug 91 TO Dec 91	October 1992	61+ vi

16. SUPPLEMENTARY NOTATION

17. COSATI CODES			18. SUBJECT TERMS (*Continue on reverse if necessary and identify by block number*)
FIELD	GROUP	SUB-GROUP	computational fluid dynamics, Large Cavitation Channel, Schiebe, cavitation head forms, laser Doppler velocimetry

19. ABSTRACT (*Continue on reverse if necessary and identify by block number*)

The objective of this project is to use computational fluid dynamics to examine the flow around three Schiebe head forms: 2 inches, 10 inches, and 20 inches in diameter. The flow around the 20-inch head form was examined experimentally in the Large Cavitation Channel by making laser Doppler velocimetry measurements. Computational analysis was used to determine the flow around all three head forms. The computational results and the experimental results were compared. The objective of the comparison was to determine if a computational model could be used to represent accurately a physical model in a test tunnel.

The results showed that both viscous and inviscid flow calculations represented the experiment well. The inviscid analysis was much less costly in time and resources while still providing useful results. Inviscid flow calculations seem to be the best choice for a preliminary prediction technique to support experimental investigations.

This report presents a description of the experimental and computational methods used, a detailed comparison of results, and an analysis of the comparison.

20. DISTRIBUTION/AVAILABILITY OF ABSTRACT ☐ UNCLASSIFIED/UNLIMITED ☑ SAME AS RPT ☐ DTIC USERS	21. ABSTRACT SECURITY CLASSIFICATION	
22a. NAME OF RESPONSIBLE INDIVIDUAL	22b. TELEPHONE (*include Area Code*)	22c. OFFICE SYMBOL Code 1521

DD Form 1473, JUN 86 *Previous editions are obsolete* SECURITY CLASSIFICATION OF THIS PAGE

S/N 0102-LF-014-6603

CONTENTS

CONTENTS (Continued)

FIGURES

FIGURES (Continued)

TABLES

ABBREVIATIONS AND SYMBOLS

B	source disk radius
CFD	computational fluid dynamics
CL	centerline
C_p	pressure coefficient
$C_{p,min}$	minimum pressure coefficient
h	vertical distance (height)
H	overall strut height
LCC	Large Cavitation Channel
LDV	laser Doppler velocimetry
NSWC	Naval Surface Warfare Center
NURB	non-uniform, rational B-spline
r	radius
R	maximum head form radius
RANS	Reynolds-averaged Navier-Stokes
V_0	free-stream velocity
V_x	longitudinal velocity
$\overline{V_x}$	mean longitudinal velocity
x	longitudinal distance
σ	standard deviation
σ_v	standard deviation of velocity
$\sigma_{\overline{v}}$	standard deviation of mean velocity

ABSTRACT

The objective of this project is to use computational fluid dynamics to examine the flow around three Schiebe head forms: 2 inches, 10 inches, and 20 inches in diameter. The flow around the 20-inch head form was examined experimentally in the Large Cavitation Channel by making laser Doppler velocimetry measurements. Computational analysis was used to determine the flow around all three head forms. The computational results and the experimental results were compared. The objective of the comparison was to determine if a computational model could be used to represent accurately a physical model in a test tunnel.

The results showed that both viscous and inviscid flow calculations represented the experiment well. The inviscid analysis was much less costly in time and resources while still providing useful results. Inviscid flow calculations seem to be the best choice for a preliminary prediction technique to support experimental investigations.

This report presents a description of the experimental and computational methods used, a detailed comparison of results, and an analysis of the comparison.

ADMINISTRATIVE INFORMATION

This work was funded by the Large Cavitation Channel project office (Code 1502), Carderock Division, Naval Surface Warfare Center, headed by Dr. Wm. Middleton and Mr. P. Yarnall, with Job Order Number 1-1502-207-03.

INTRODUCTION

The recent development of the Large Cavitation Channel (LCC) has brought about a chance to implement state-of-the-art instrumentation and experimental techniques. Accurate and intricate experimental investigations of flow phenomena are made feasible by these procedures. Laser Doppler velocimetry (LDV) is among these techniques. Computational fluid dynamics (CFD) is another state-of-the-art discipline that is now leaving the "research-only" stage and entering practical use. Computational techniques include viscous flow codes and

inviscid flow codes. Recent and on-going improvements to these algorithms have enabled them to be used for increasingly accurate estimates of flow phenomena.

The LCC presents an opportunity to exploit the capabilities of these technologies, LDV and CFD, and use them to complement each other. The primary benefits are two-fold. First, the technologies allow much more detailed and complicated investigations. Second, the traditional experimental method is made more efficient and reliable by providing a system for more careful planning and execution of measurements.

The ultimate goal of this integration is to develop a system where computations are used as a preliminary prediction technique for flow characteristics. Physical investigations would concentrate in areas of interest identified by the early calculations. A computational-to-experimental correlation could then be determined, and the calculations revised to represent the actual flow more accurately. A database of correlations would be constantly updated, leading to increased accuracy in future preliminary predictions. Further investigations of the same model, including small changes in model shape, appendages, test condition, etc., could be examined computationally, reducing the use of costly experimental resources and facilities.

Such a system cannot be fully implemented at this time. The data base to make accurate and reliable correlations has not been gathered yet. Nor are the intricacies of the techniques involved currently understood to the degree necessary to use their potential fully. Still, the experience to use these techniques must be gained when possible, so that an integrated computational-experimental system can be implemented without a long delay. The growing costs in time and money for experiments push toward the use of a more efficient system with increasing power. This project represents the first step toward an integrated experimental-computational analysis system.

MODEL AND TEST FACILITY DESCRIPTION

The three models examined consisted of a Schiebe head form forward of an axisymmetric

body with a tapered tail. The Schiebe series of bodies was developed by calculating the potential flow around a source disk in a uniform field, yielding a minimum pressure coefficient ($C_{p,min}$). As the source disk radius (B) is decreased, the minimum pressure coefficient on the head form surface increases, with a point source (B=0) yielding a minimum pressure coefficient of -0.33. The series of bodies is classified based on minimum pressure coefficient and geometrically scaled to the desired size.[1*] The three models examined had geometrically similar Schiebe head forms with a minimum pressure coefficient of -0.75. The head forms were 2 inches, 10 inches and 20 inches in diameter. Table 1 gives the non-dimensional offsets of the $C_{p,min}$=-0.75 Schiebe head form.

The head form was followed by a body of revolution in each case. Vertical tail fins were added to the 10-inch and 20-inch bodies to minimize bending moments on the support strut. The small cross-section and long, slender shape of the 2-inch model was stable without fins. All three models were mounted on the same ogive strut. Figure 1 shows profile drawings of these models.

The experimental analysis was undertaken in the test tunnel at the Large Cavitation Channel (LCC), a Carderock Division, Naval Surface Warfare Center (NSWC) detachment in Memphis, Tennessee. The test section in the tunnel is 40 feet long, and 10 feet by 10 feet in cross-section, with 1.25 foot notches in each corner. Windows are located on each surface around the tunnel test section throughout the length. The windows on the top and bottom are obstructed by ceiling plates and an acoustic trough, respectively. Excellent visibility is afforded to the tunnel centerline along the entire length from the test platform. The structure around the windows limits the accessibility of an orthogonal line-of-sight to the model, which is necessary when making laser Doppler velocimetry measurements.

In the computational analysis, the bodies were arranged such that the model axis was

---

* References are listed on page 61.

incident with the tunnel centerline. In the physical experiment of the 20-inch model, the longitudinal axis was aligned about one-half degree nose down, and one-half degree yawed away from the control room, but very close to the tunnel centerline.

COMPUTATIONAL ANALYSIS

The computational analysis process involves many steps. The numerical models must be developed, much like physicals models are developed. A numerical representation must be generated, suitable to the particular type of calculations being performed. The calculations are made, and the solution must be iterated until reasonable results are achieved. Finally, the results must be presented in a meaningful form. This process involves many computer programs and tools. Figure 2 shows an overview of this process. The basics of this process are described below. A detailed description of the procedure appears in Appendix A.

GEOMETRIC MODELLING

To begin the computational analysis, numerical models were developed. Representations of the cavitation head form models, the strut, and the LCC test section were generated from assembly drawings and offsets. Three-dimensional numerical surfaces representing the desired physical model were generated. As the surfaces were defined, a grid was distributed over the surface. Shaded pictures of these surfaces were generated, as shown in Figure 3. These pictures are commonly used for presentations, discussions, and visual inspections.

As is common for symmetrical forms, only half-models were developed for the computations. For the viscous flow analysis, a model of the 20-inch test body was generated with the strut and tunnel walls. For the inviscid flow computations, a model of the 20-inch body and strut was generated both with and without the tunnel walls. The tunnel walls did not influence the flow noticeably in the primary area of interest (i.e., the head form), as explained later. Therefore, the inviscid panel models for the 2-inch and 10-inch bodies were generated with

the strut but without the tunnel walls.

VISCOUS FLOW CALCULATIONS

Grid Generation

A three-dimensional, multi-block, volume grid was developed around the surface grid. A block structure was developed around the desired geometry. A sample of the block structure is shown in Figure 4. The heavy lines in the figure represent block edges. The half-model is clearly visible, as is the outline of the tunnel.

The topology of the blocks was defined, as was the connectivity of the blocks. Figure 5 shows selected block faces from the grid developed for the 20-inch model in the tunnel. The heavy lines in the figure again represent block edges, while the thin lines show the grids on the block faces. For clarity, only a few block faces are shown.

Once the face grids were defined, the coordinates of the points on the interior of each block were interpolated. These points outline cells, or three-dimensional volumes. The cells were checked to ensure that their orientation was consistent (i.e., in a right-handed coordinate system). Iterations of the grid generation were made to achieve an acceptable three-dimensional volume grid with a relatively smooth and properly oriented grid distribution.

The details for developing a block structure and grid distribution vary greatly from case to case, and are sometimes based heavily on trial-and-error. Each model has different properties which define various characteristics of the block structure and grid distribution. Hopefully, early determination these characteristics can be made easier in the future. For practical application, criteria must be developed to help guide the grid generation. The criteria will be based on the collective and continuing experience from successfully developed grids. In addition, the constant refinement of existing software, along with the development of new software and hardware, facilitates the process of numerical model generation.

The 20-inch body was modelled with the vertical tail fins and mounted on the strut. The

inner boundary of the volume grid was the body surface and tunnel centerline, and the outer boundaries were the tunnel walls. For computational reasons, the grid was extended forward of the model by one-half a body length, and aft by a full body length. Figure 4 shows the grid outline well.

Solution Technique

A steady-state, incompressible viscous flow calculation was made, using the three-dimensional Reynolds-averaged Navier-Stokes (RANS) equations.

Since single grid can require a total of 250 to 350 hours of computer time to calculate a final solution, viscous flow analyses are potentially expensive in computer time. Most of this time is spent in the iterative process of refining the grid for an improved flow solution. The cost of computer time and equipment corresponds to the material and facilities costs in physical tests. Viscous flow calculations currently can be competitive in cost to physical model tests. The costs of computational analysis become more favorable as faster and less expensive computers become available.

Examining changes in model configuration is often less costly when done computationally. As long as the block topology and grid distribution does not need to change radically, subsequent model configurations and conditions often take only 100 to 150 hours total computer time. Physical model experiments generally require as much time for each configuration, which can monopolize facilities, further increasing costs. A parametric study of a hull form or appendage suite can be very costly when tested physically. The same study can be much more extensive and affordable when performed computationally. Preliminary and/or follow-up physical tests can be used to verify computational results, thereby ensuring the accuracy of the analysis.

INVISCID FLOW CALCULATIONS

Model Generation

Inviscid flow calculations are typically made for one or more panelled surfaces. The panelled surfaces are generally the surface grids developed earlier, but with a refined distribution. Figure 6 shows the panel distribution used for the 20-inch model and strut. Note the concentration of panels about the area of high curvature in the head form.

The 20-inch model was generated both with and without the tunnel walls. After viewing the results, it was determined that the tunnel walls did not affect the flow over the head form in the inviscid flow solution. The tunnel walls only influenced the flow along the strut and near the model-strut interface. The tunnel walls were not included in the panel models for the 2-inch and 10-inch head forms to reduce computation time.

Solution Technique

The inviscid flow calculations were made for the head form models. An inviscid flow solution can take anywhere from 2 to 5 minutes of computational time. Even multiple iterations while refining the panel distribution do not involve much computer time. Viscous flow effects, such as turbulence and separation, are not accounted for by inviscid flow analyses. These effects are often very significant, and cannot always go unexamined. On the other hand, inviscid flow programs have the advantage of including free-surface effects more easily.

Some CFD codes are hybrids: the program uses different solution techniques on different sections of the model. This arrangement has both advantages and disadvantages. No programs of this type were evaluated during the course of this investigation. They are mentioned only for completeness.

PRESENTATION OF RESULTS

The way in which computational results are presented can be nearly as important as the

calculations themselves. Tools are available to display the results in many formats. One format is three-dimensional color or shaded pictures. Two figures show results from the viscous flow calculations. Figure 7 shows a plot of pressure coefficients on the 20-inch model and strut, while Figure 8 shows particle traces around the same model. For the particle trace, three particles were released near the head form surface. Their traces were computed forward and backward in time, showing where the particles were headed, as well as where they had been. Three particles were also released just forward of the upper fin leading edge. Their traces were computed aft only.

Results were also plotted in two-dimensional formats using various commercially available graphing/plotting packages. Three-dimensional pictures are often not the most useful method of presenting results for computations. Two-dimensional graphs are frequently used in cases where specific quantities are more important than general trends, or cases where specific comparisons must be made, as was the case in comparing the velocity profiles and pressure coefficients in this report.

EXPERIMENTAL ANALYSIS

SETUP

The laser Doppler velocimetry (LDV) measurements were conducted only for the 20-inch model due to time constraints on the Large Cavitation Channel (LCC) facility.

The locations of test points for the LDV system are limited by tunnel structure, lens focal length, and the limits of the traverse mechanism. In this case, the test points were restricted to the volume around the head form. The physical extents of the traverse mechanism restricted movement past the pair of windows at the forward end of the model. No points could be located immediately forward of the stagnation point due to obstructing window structure. The focal length of the lens allowed test points to be located slightly past the centerplane of the tunnel. Figure 9 describes these limits graphically.

A test matrix was developed to examine several areas around the head form at three different speeds. The matrix allowed for testing above and below the head form in the centerplane, as well as around the model girth. A forward profile and a profile from the model to the near tunnel wall were also planned. About 400 samples were taken at each test point. Table 2 describes the experimental test matrix.

TEST PROCEDURE

For this particular LDV setup, it was determined that approximately 350 samples at each point must be collected before the mean velocity becomes a steady value, as shown in Figure 10. The two groups of samples shown in the figure represent one highly turbulent point (near the tunnel wall) and one point with low turbulence (near the model surface).* Note that even after only 100 samples, the mean is quite steady (within one standard deviation of the mean velocity).

The system installed at the LCC was used in a one-component back-scatter mode for this test. One-component mode indicates that only the longitudinal component of velocity (V_x) was measured. The receiving optics used were located in the same housing as the transmitting optics, so that only light bouncing back toward the lens, or back-scatter, was received. The transmitting lens has a fixed focal length, and was mounted on a three-axis traverse. The traverse allowed the lens to be moved in any direction, and therefore the test point location could be moved in three dimensions.

A discussion of LDV theory and operation is beyond the scope of this report, but is readily available from many sources, including Durst *et al.*[2]

---

* Turbulence in any direction is defined as the standard deviation of the velocity in that direction divided by the mean longitudinal velocity, or

$$\%turbulence = \frac{\sigma_V}{V_x} \times 100\% \ .$$

DATA ANALYSIS

The data were analyzed by averaging the valid samples for each point (400 samples in most cases). Samples outside four standard deviations from the mean were not included. This filtering removed outliers* without affecting samples in the expected distribution. Figure 11 shows examples of the distribution of samples as well as showing the filter criteria. A high and a low turbulence point are shown. The distributions of other points were similar.

The resulting mean velocities were graphed as velocity profiles. Three velocity profiles are shown in Figure 12. Tabulated results for all profiles are shown in Table B-1 of Appendix B.

RESULTS AND DISCUSSION

SCHIEBE RESULTS

A potential flow analysis was used by Schiebe to determine the pressure distribution on the body surface.[1] Since the body is axisymmetric, the pressure coefficients vary only with longitudinal distance from the stagnation point. The results from Schiebe are shown in Table 3.

INVISCID FLOW

Inviscid Flow versus Schiebe

Figure 13 shows pressure coefficient versus longitudinal distance from the stagnation point for the 20-inch head form model, along with the Schiebe results. These pressure coefficients are also listed in Table 4. The coefficients were computed along the side of the models at 90 degrees from the upper edge and at the lower edge along the centerline. Since the side of the model is well removed from either the strut or the centerline (a mathematical boundary), the results at the side would be expected to best match the results from Schiebe (which are for an unappended head form). The comparison is very favorable for both the side and

* Outliers are "readings that appear to be significantly out of line with the other readings."[3]

the lower edge, however. Figure 13a shows the pressure coefficients along the surface of the head form, while Figure 13b extends the graph to show the length of the model. The results from Schiebe were calculated for the head form only (i.e., no strut or fins.) The results along the lower edge are not relevant to the comparison in way of the tail fins, since there is no fin at the side of the model.

Wall Effects

Figure 14 compares the pressure coefficients of the 20-inch half-model for the two configurations tested: with and without the tunnel walls. Figure 14a shows that there is no apparent wall effect at the side of the model, while Figure 14b shows the pressure coefficients on the strut centerline. In the first graph, the wall effect can be seen as a slight offset in way of the strut. The second graph shows a difference in pressure coefficient of about 0.04 at the bottom of the strut centerline. These data are also presented in Table 5.

This slight effect on the model is important to consider because the wall definition requires about the same number of panels as the model and strut combined, and therefore the solution takes about twice as much computer time. The small effect at the strut does not seem to influence the results on the head form appreciably. Since the 20-inch head form will have the greatest wall effect of the three head form models, it is reasonable to assume that no walls need to be modelled for the 2-inch and 10-inch head forms.

This minor wall effect must be taken in context, however. This axisymmetric model was 20 inches in diameter in a tunnel 10 feet by 10 feet in cross-section. The ratio of cross-sectional areas (i.e., blockage factor) is only $1/44$. In addition, the model was mounted so that its surface was slightly over five times the head form radius from the tunnel walls. A test of wall effect should be carried out for models of equal or greater blockage factor or for models mounted closer to walls. Of course, surface ship models mounted at the ceiling plate should always be modelled with tunnel walls.

The wall effect is significant on the strut. Therefore, calculations for models in which the flow on or around the strut are important should include walls. Likewise, the strut effect is significant on the model. Mounting hardware and objects near or on the body can significantly influence the flow characteristics and should always be modelled.

Boundary Condition Effects

Figure 15 presents the half-model results at the lower edge of the model and corresponding results from a bare (unappended) 20-inch full-model. The numerical definition of the full-model starts and ends along the upper edge of the model, meaning that the lower edge is 180 degrees removed from any mathematical boundary. The mathematical boundary condition seems to have little effect on the solution.

Figure 13 can also be used to examine boundary condition effects. The results at the side of the model (90 degrees removed from a boundary) and the lower edge (at a boundary) agree closely. The upper edge of the model was not considered due to the presence of the strut.

This consistency is an indication that the mathematical boundary condition does not adversely affect the inviscid flow calculation results. The full-model has twice the number of panels and requires about twice the computer time. The half-model is a satisfactory representation. Unless otherwise stated, references elsewhere in this report to the model refer to the half-model.

Scale Effects

Figure 16 shows the pressure coefficients for each of the head forms at the side of each model. The results for all three head forms agree very well with each other, as well as with the Schiebe results. Inviscid flow theory deals primarily in non-dimensional values, and would not be expected to show any discrepancy between the head forms. These results are tabulated in Table 6.

It should be observed that the panels for the three head forms were not distributed similarly, as shown by the differing locations of the data points in the figure. The inviscid flow calculation results do not vary significantly with small differences in panel distribution. The ability to achieve consistent results when varying panel distributions is important for a preliminary prediction technique.

VISCOUS FLOW

Viscous Flow versus Schiebe

Figure 17 shows the pressure coefficients for the viscous flow calculation, plotted with the inviscid flow calculation results and results from Schiebe. The viscous flow calculation results are also listed in Table 7. The pressure coefficients are compared at the side of the 20-inch head form. The results of the viscous flow calculation are not as close to the Schiebe results as are the inviscid flow calculation results. However, the results show the correct trend and the magnitudes seem reasonable.

A basic difficulty in working with viscous flow calculations is that the results are often dependant on grid distribution. This dependence inhibits the usefulness of viscous flow calculations as a preliminary prediction technique. Without a prior estimate, it is difficult to determine whether the viscous flow calculation results are reasonable indicators of the actual flow, or merely the results of a particular grid distribution. In this case, it would seem that further refinement of the grid in the forward area of the head form would be important if the grid results were to be used for other investigations. One example of such investigations would be a parametric study to optimize the pressure distribution on the head form. The results are close enough to indicate that reiteration of the grid might yield more accurate results, and the scope of this investigation does not warrant further refinement.

Boundary Condition Effects

Figure 18 shows pressure coefficient versus longitudinal distance from the stagnation point for viscous flow calculations, similar to the investigation presented in Figure 13 for inviscid flow calculations. The results at the side and at the lower edge are compared. The comparison for the viscous flow calculation results are not as favorable. The lower edge boundary condition seems not to represent the symmetric plane very well in the head form area. Past the head form section (i.e., $x/L > 5$), the side and lower edge results agree quite well. The conclusion is that if the area near a mathematical boundary is of particular interest, full-body models should be considered. The trade-off is computational cost and speed versus accuracy.

The full-body model was not tested for the viscous flow calculations due to time and cost considerations. Likewise, wall effects and scale effects were not examined for viscous flow calculations.

Viscous Flow versus Experiment

Figure 19 shows a comparison of experimental results and viscous flow calculation results. The results are similar in trend and magnitude except near the model surface and tunnel walls. The agreement is quite reasonable.

In each of the profiles compared, it appears that the boundary layer growth in the viscous flow calculation is too large. The turbulence modelling in the viscous flow calculations uses an empirical correlation. The representation can be changed, although sufficient experimental data must be available to guide the change. The results of these investigations and future investigations can be used to compile a data base for increasing the accuracy of the empirical correlation.

The modification of empirical correlations is not trivial, but could be used if closer agreement between the numerical and the physical model was necessary. The cost of developing a data base and making a modification was not justified for this investigation. The cost would be

justified for long term computational support of physical experiments. Also, as more of a data base is gathered over time, the cost of applying a modification of this type decreased, while the improved accuracy increases, both due to a larger base or experience to guide the change.

CONCLUSIONS AND RECOMMENDATIONS

The results of this project indicate that accurate representations of physical models can be achieved with currently available computational tools and techniques. Computational fluid dynamics can reasonably support physical experiments, and will become more useful in that role as further experience is gained.

The inviscid flow calculations provide meaningful, reasonable data at a relatively low cost in time and resources. The calculations are stable with regard to panel distribution. These characteristics enable the inviscid flow model to be a competent preliminary prediction technique for physical experiments in a tunnel.* Inviscid flow calculations can provide the engineer with vital information prior to the experiment.

For many cases, a half-model representation with mounting hardware is sufficient for inviscid flow calculations. The tunnel walls may not have to be modelled. Before these assumptions are made, however, areas of interest should be identified and the effects of these assumptions considered. These assumptions have the potential to reduce computational time, but could adversely affect the results in certain situations.

The viscous flow calculations can provide different information than inviscid flow calculations, but require more time and resources. Results are sensitive to grid distribution, making viscous flow calculations poorly suited to be used as a preliminary prediction technique at the current time. The development of grid distribution criteria is crucial to the practical

---

* No effort was made to validate free surface modelling capabilities of the inviscid flow calculations, and therefore no conclusions can be made as to the proficiency of predicting experimental flow in non-tunnel environments (e.g., towing tanks).

application of viscous flow calculations. Experience and improvements in the techniques will certainly make a difference in the future. The results from this investigation add to the experience base and can be used for guidance in future work.

Currently, viscous flow calculations seem best suited to parametric studies. A baseline grid distribution can developed and results verified with experiments or other prediction techniques. Parametric changes could then be made to the grid without requiring the block structure to be significantly altered. Also, cases where inviscid flow calculations will not yield the necessary information (e.g., separated flow characteristics) are candidates for examination using viscous flow calculations.

Experimental results are important to help guide the empirical techniques used in turbulence modelling for viscous flow computations. For example, experimental data should be gathered to determine boundary layer characteristics and growth. Once enough information is available, the empirical turbulence model currently used can be updated to more accurately represent the characteristics of the boundary layer in a tunnel. Correlation with experiments would be improved, increasing the usefulness of viscous flow calculations for experimental support.

Based on these conclusions, the authors make the following recommendations:

- Inviscid flow calculations should be used to develop preliminary predictions of flow characteristics prior to performing experiments. The cost of the calculations is offset by the availability of preliminary estimates prior to the experiment. The reliability of these calculations seems to justify their use.
- Whenever time and resources permit, viscous flow calculations should be performed in conjunction with the experiment to aid in the development of tools and techniques. The experience will help develop grid generation guidelines, and the correlation with the experimental results will help refine empirical techniques used

in viscous flow calculations. These developments will make viscous flow calculations less costly and more reliable in the future for experimental and design support.

- The integration of computational fluid dynamics and physical experimental techniques should be continued in order to improve the overall experimental technique. This is crucial to the modernization of experimentation.

ACKNOWLEDGMENTS

The authors would like to thank Paul Impelluso, Gerald Smith, and Steven Fisher of the David Taylor Model Basin for their help in the numerical analysis and the preparation of this report. The authors would also like to thank Steven Ceccio of the University of Michigan for his advice and guidance with the experiment.

Table 1. Schiebe head form offsets for the $C_{p,min}$=-0.75 head form.

Longitudinal distance from stagnation point (x/R)	Radius (r/R)
0.00000	0.00719
0.00000	0.01437
0.00000	0.02156
0.00000	0.02875
0.00000	0.03593
0.00252	0.14853
0.00503	0.20863
0.00754	0.25373
0.01005	0.29098
0.01257	0.32307
0.02513	0.44066
0.03769	0.51915
0.05025	0.57508
0.06281	0.61532
0.07537	0.64424
0.08793	0.66549
0.10049	0.68196
0.11305	0.69549
0.12561	0.70711
0.14561	0.72299
0.16561	0.73666
0.18561	0.74876
0.20561	0.75968
0.22561	0.76964
0.24561	0.77882
0.26561	0.78733
0.28561	0.79527
0.30561	0.80271
0.32561	0.80970
0.34561	0.81630
0.36561	0.82253
0.38561	0.82844
0.40561	0.83405
0.42561	0.83939
0.52561	0.86263
0.62561	0.88134
0.72561	0.89671
0.82561	0.90948
0.92561	0.92021
1.02561	0.92930
1.12561	0.93704
1.52561	0.95870
1.92561	0.97131
2.32561	0.97913
2.72561	0.98424
3.12561	0.98773
3.52561	0.99020
3.92561	0.99201
4.32561	0.99337
4.72561	0.99441
5.12561	0.99523

All values are non-dimensional by maximum head form radius.

Table 2. Experimental test matrix.

Profile		Nominal tunnel velocity		
		13.6 knots	22.4 knots	29.2 knots
Along lower edge,	forward of $C_{p,min}$		•	
	4 in. aft			
	8 in. aft		•	
	16 in. aft			
Forward of stagnation point				•
Around girth,	at upper edge		•	•
8 in. aft	at 45° above CL		•	•
	at CL		•	•
	at 45° below CL		•	•
	at lower edge		•	•
Along upper edge,	forward of $C_{p,min}$			
	4 in. aft			•
	8 in. aft			
	16 in. aft		•	
At CL, from model to tunnel wall		•	•	•

All distances referenced to stagnation point.

Angles are referenced from horizontal.

Table 3. Pressure coefficients on Schiebe head form ($C_{p,min}$=-0.75) from potential flow theory.

Longitudinal distance from stagnation point (x/R)	Pressure coefficient (C_p)
0.00000	0.99890
0.00000	0.99930
0.00000	0.99960
0.00000	0.99982
0.00000	0.99996
0.00252	0.98048
0.00503	0.95995
0.00754	0.93837
0.01005	0.91560
0.01257	0.89158
0.02513	0.74947
0.03769	0.56043
0.05025	0.31004
0.06281	-0.00163
0.07537	-0.32280
0.08793	-0.56007
0.10049	-0.68488
0.11305	-0.73585
0.12561	-0.75001
0.14561	-0.74129
0.16561	-0.71918
0.18561	-0.69385
0.20561	-0.66857
0.22561	-0.64444
0.24561	-0.62174
0.26561	-0.60050
0.28561	-0.58062
0.30561	-0.56198
0.32561	-0.54447
0.34561	-0.52797
0.36561	-0.51238
0.38561	-0.49761
0.40561	-0.48359
0.42561	-0.47024
0.52561	-0.41187
0.62561	-0.36411
0.72561	-0.32402
0.82561	-0.28983
0.92561	-0.26035
1.02561	-0.23472
1.12561	-0.21232
1.52561	-0.14631
1.92561	-0.10503
2.32561	-0.07811
2.72561	-0.05989
3.12561	-0.04713
3.52561	-0.03793
3.92561	-0.03111
4.32561	-0.02593
4.72561	-0.02192
5.12561	-0.01876

Distances are non-dimensional by maximum head form radius.

Pressure coefficients are referenced to the uniform flow.

Table 4. Inviscid flow calculation results for the 20-inch head form.

Longitudinal distance from stagnation point (x/R)	Pressure coefficient (C_p)	
	At side	At lower edge
0.000	1.0000	1.0000
0.000	0.9996	0.9995
0.000	0.9988	0.9986
0.000	0.9965	0.9963
0.001	0.9933	0.9930
0.001	0.9881	0.9877
0.003	0.9806	0.9801
0.004	0.9694	0.9689
0.006	0.9521	0.9512
0.009	0.9265	0.9255
0.013	0.8912	0.8899
0.019	0.8371	0.8354
0.026	0.7553	0.7534
0.036	0.6243	0.6221
0.049	0.4085	0.4049
0.068	0.0117	0.0071
0.098	-0.5293	-0.5345
0.139	-0.7352	-0.7401
0.185	-0.6875	-0.6940
0.232	-0.6297	-0.6366
0.276	-0.5871	-0.5930
0.316	-0.5537	-0.5581
0.353	-0.4853	-0.4888
0.386	-0.4312	-0.4378
0.415	-0.4636	-0.4682

Longitudinal distance from stagnation point (x/R)	Pressure coefficient (C_p)	
	At side	At lower edge
0.439	-0.4682	-0.4638
0.461	-0.4339	-0.4248
0.479	-0.4524	-0.4448
0.495	-0.4462	-0.4430
0.515	-0.4079	-0.4057
0.569	-0.3776	-0.3736
0.676	-0.3308	-0.3292
0.835	-0.2921	-0.2889
1.041	-0.2362	-0.2312
1.289	-0.1883	-0.1842
1.573	-0.1545	-0.1506
1.887	-0.1309	-0.1263
2.222	-0.0827	-0.0777
2.569	-0.0616	-0.0575
2.922	-0.0728	-0.0694
3.269	-0.0717	-0.0689
3.604	-0.0639	-0.0617
3.918	-0.0527	-0.0516
4.203	-0.0478	-0.0481
4.452	-0.0487	-0.0517
4.659	-0.0477	-0.0533
4.818	-0.0412	-0.0487
4.927	-0.0338	-0.0458
4.982	-0.0231	-0.0287
5.002	-0.0245	-0.0200

Distances are non-dimensional by maximum head form radius.

Pressure coefficients are referenced to the uniform flow.

Table 5. Inviscid flow calculation results for the 20-inch head form with and without tunnel walls.

Table 5a. Pressure coefficients on the head form surface.

Longitudinal distance from stagnation point (x/R)	Pressure coefficient (C_p)	
	Head form with walls	Head form without walls
0.000	0.9999	1.0000
0.000	0.9996	0.9996
0.000	0.9988	0.9988
0.000	0.9966	0.9965
0.001	0.9932	0.9933
0.001	0.9877	0.9881
0.003	0.9803	0.9806
0.004	0.9694	0.9694
0.006	0.9521	0.9521
0.009	0.9265	0.9265
0.013	0.8906	0.8910
0.019	0.8365	0.8370
0.026	0.7550	0.7553
0.036	0.6233	0.6243
0.049	0.4063	0.4087
0.068	0.0099	0.0126
0.098	-0.5319	-0.5277
0.139	-0.7407	-0.7342
0.185	-0.6935	-0.6882
0.232	-0.6338	-0.6302
0.276	-0.5943	-0.5874
0.316	-0.5586	-0.5509
0.353	-0.4867	-0.4822
0.386	-0.4372	-0.4344
0.415	-0.4729	-0.4648

Longitudinal distance from stagnation point (x/R)	Pressure coefficient (C_p)	
	Head form with walls	Head form without walls
0.439	-0.4775	-0.4647
0.461	-0.4384	-0.4306
0.479	-0.4542	-0.4490
0.495	-0.4454	-0.4405
0.515	-0.4027	-0.3996
0.569	-0.3781	-0.3732
0.676	-0.3375	-0.3296
0.835	-0.2978	-0.2891
1.041	-0.2398	-0.2314
1.289	-0.1935	-0.1840
1.573	-0.1606	-0.1498
1.887	-0.1379	-0.1263
2.222	-0.0883	-0.0787
2.569	-0.0677	-0.0577
2.922	-0.0828	-0.0691
3.269	-0.0836	-0.0684
3.604	-0.0772	-0.0616
3.918	-0.0684	-0.0512
4.203	-0.0657	-0.0479
4.452	-0.0685	-0.0515
4.659	-0.0701	-0.0531
4.818	-0.0646	-0.0482
4.927	-0.0621	-0.0457
4.982	-0.0389	-0.0253
5.000	-0.0363	-0.0224

Distances are non-dimensional by maximum head form radius.

Pressure coefficients are referenced to the uniform flow.

Table 5. (Continued).

Table 5b. Pressure coefficients along the strut centerline.

Vertical distance along strut centerline (h/H)	Pressure coefficient (C_p)	
	Strut with walls	Strut without walls
Bottom 0.00	-0.5161	-0.4891
0.10	-0.5399	-0.5120
0.20	-0.5421	-0.5121
0.30	-0.5323	-0.5002
0.40	-0.5282	-0.4913
0.50	-0.5248	-0.4830
0.60	-0.5164	-0.4685
0.70	-0.5029	-0.4454
0.80	-0.4944	-0.4203
0.90	-0.4867	-0.3862
Top 1.00	-0.4604	-0.3248

Vertical distances are non-dimensional by overall strut height.

Pressure coefficients are referenced to the uniform flow.

Table 6. Inviscid flow calculation results for the 2-inch and 10-inch head forms.

Longitudinal distance from stagnation point (x/R)	Pressure coefficient (C_p)	
	2-inch head form	10-inch head form
0.000	0.9999	1.0000
0.000	0.9996	0.9996
0.000	0.9988	0.9988
0.000	0.9966	0.9965
0.001	0.9932	0.9933
0.001	0.9877	0.9881
0.003	0.9803	0.9806
0.004	0.9694	0.9694
0.006	0.9521	0.9521
0.009	0.9265	0.9265
0.013	0.8906	0.8910
0.019	0.8365	0.8370
0.026	0.7550	0.7553
0.036	0.6233	0.6243
0.049	0.4063	0.4087
0.068	0.0099	0.0126
0.098	-0.5319	-0.5277
0.139	-0.7407	-0.7342
0.185	-0.6935	-0.6882
0.232	-0.6338	-0.6302
0.276	-0.5943	-0.5874
0.316	-0.5586	-0.5509
0.353	-0.4867	-0.4822
0.386	-0.4372	-0.4344
0.415	-0.4729	-0.4648
0.439	-0.4775	-0.4647
0.461	-0.4384	-0.4306
0.479	-0.4542	-0.4490
0.495	-0.4454	-0.4405
0.515	-0.4027	-0.3996
0.569	-0.3781	-0.3732
0.676	-0.3375	-0.3296
0.835	-0.2978	-0.2891
1.041	-0.2398	-0.2314
1.289	-0.1935	-0.1840
1.573	-0.1606	-0.1498
1.887	-0.1379	-0.1263
2.222	-0.0883	-0.0787
2.569	-0.0677	-0.0577
2.922	-0.0828	-0.0691
3.269	-0.0836	-0.0684
3.604	-0.0772	-0.0616
3.918	-0.0684	-0.0512
4.203	-0.0657	-0.0479
4.452	-0.0685	-0.0515
4.659	-0.0701	-0.0531
4.818	-0.0646	-0.0482
4.927	-0.0621	-0.0457
4.982	-0.0389	-0.0253
5.000	-0.0363	-0.0224

Distances are non-dimensional by maximum head form radius.

Pressure coefficients are referenced to the uniform flow.

Table 7. Viscous flow calculation results for the 20-inch model.

Longitudinal distance from stagnation point (x/R)	Pressure coefficient (C_p)	
	At side	At lower edge
0.000	3.2095	4.8852
0.001	2.9300	4.2880
0.003	2.0230	3.8952
0.006	1.3683	2.5691
0.011	0.8734	1.5403
0.017	0.7396	0.8620
0.024	0.5729	0.4874
0.034	0.2865	0.4268
0.048	-0.1212	0.3668
0.069	-0.5559	0.0101
0.102	-0.9352	-0.4142
0.151	-1.1045	-0.7568
0.209	-1.0382	-1.0106
0.280	-0.9125	-1.1480
0.369	-0.7634	-1.2256
0.477	-0.6443	-1.2399
0.602	-0.5790	-1.0810
0.739	-0.5483	-0.8974
0.884	-0.5260	-0.6793
1.028	-0.4812	-0.5049
1.167	-0.4041	-0.3135
1.294	-0.2999	-0.1855
1.414	-0.2072	-0.0728
1.539	-0.1421	0.0663
1.676	-0.1028	0.1639
1.823	-0.0781	0.2770

Longitudinal distance from stagnation point (x/R)	Pressure coefficient (C_p)	
	At side	At lower edge
1.980	-0.0700	0.3628
2.146	-0.0632	0.4025
2.320	-0.0538	0.4603
2.500	-0.0476	0.4629
2.683	-0.0469	0.4363
2.869	-0.0500	0.4093
3.055	-0.0548	0.3616
3.238	-0.0620	0.3239
3.416	-0.0691	0.2953
3.588	-0.0683	0.2623
3.752	-0.0559	0.2378
3.907	-0.0404	0.2270
4.052	-0.0383	0.2222
4.185	-0.0631	0.2188
4.308	-0.1081	0.2161
4.420	-0.1452	0.2140
4.521	-0.1552	0.2145
4.612	-0.1434	0.2175
4.693	-0.1220	0.2073
4.765	-0.1017	0.1467
4.828	-0.0912	0.0443
4.884	-0.0567	-0.1060
4.933	0.0408	-0.3337
4.976	0.1336	-0.4517
5.016	0.1984	-0.3373

Distances are non-dimensional by maximum head form radius.

Pressure coefficients are referenced to the uniform flow.

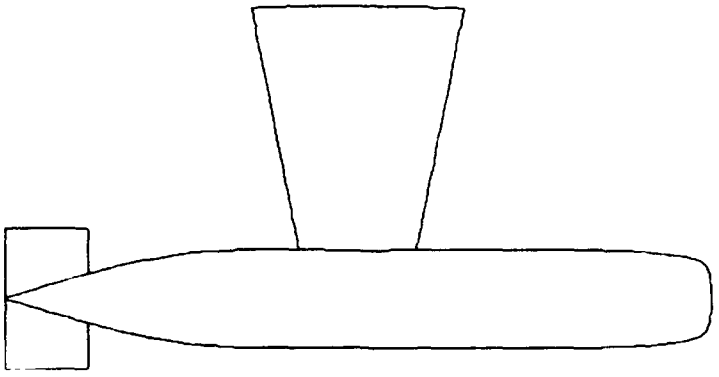

Fig. 1a. 20-inch head form model and strut.

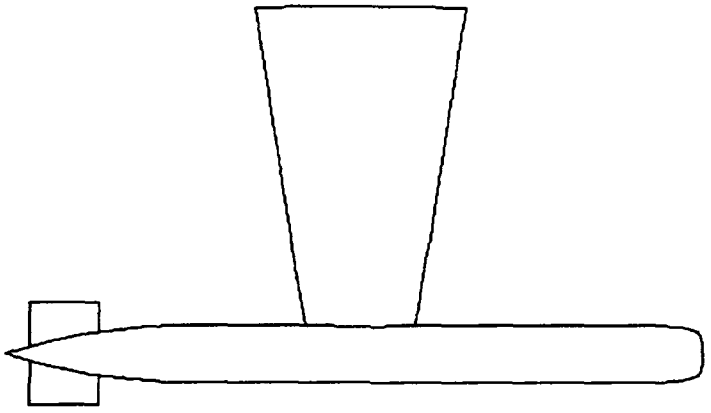

Fig. 1b. 10-inch head form model and strut.

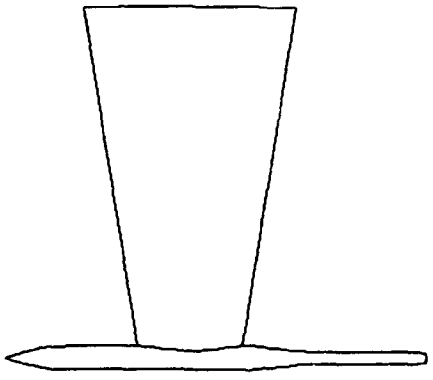

Fig. 1c. 2-inch head form model and strut.

Fig. 1. Profile drawings of the 20-inch, 10-inch, and 2-inch head form models.

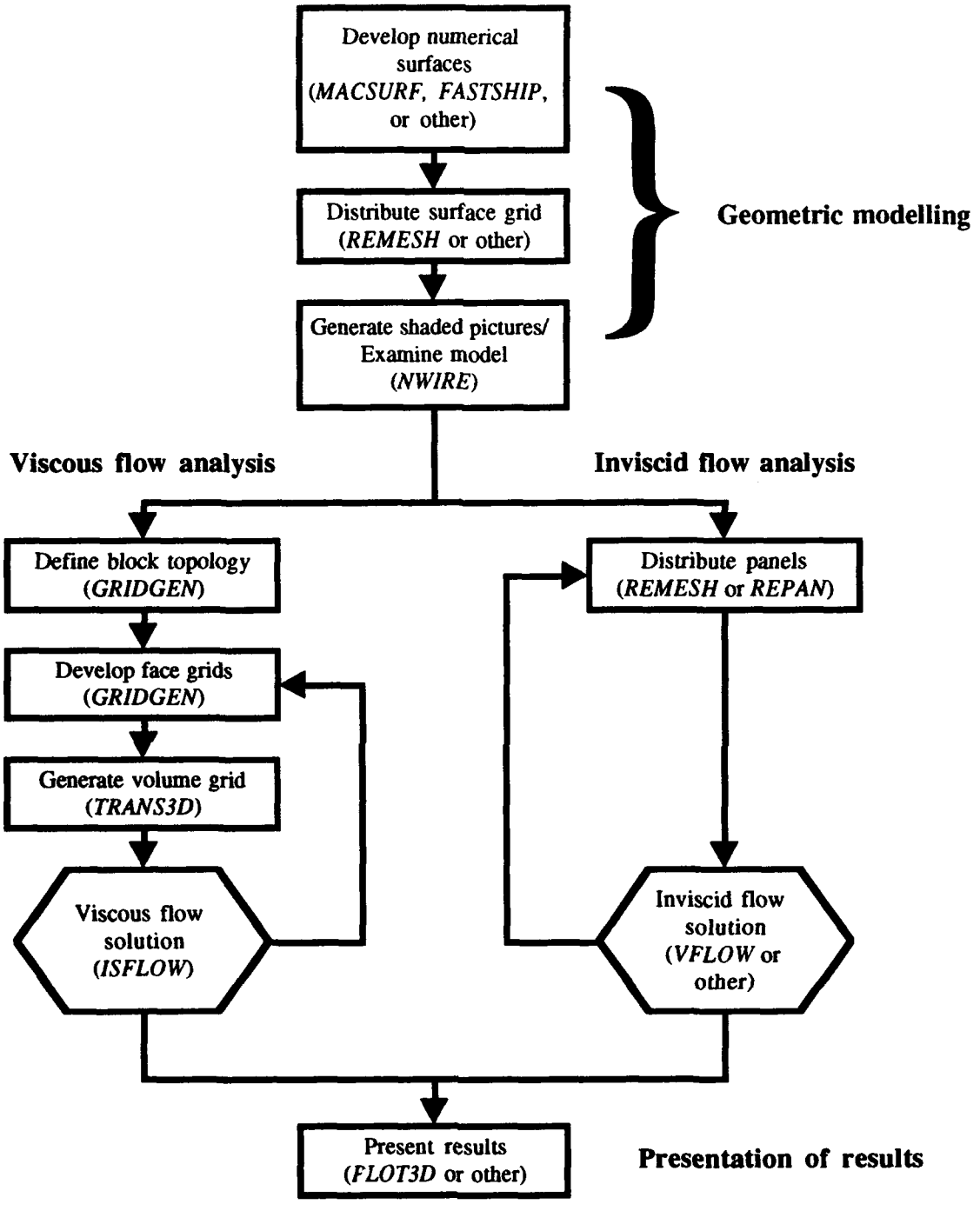

Fig. 2. Computational analysis processes and associated computer programs.

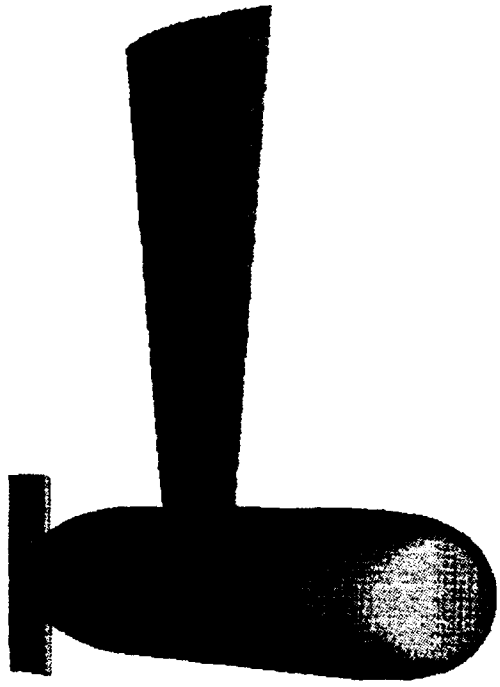

Fig. 3. Shaded picture of the 20-inch model and strut.

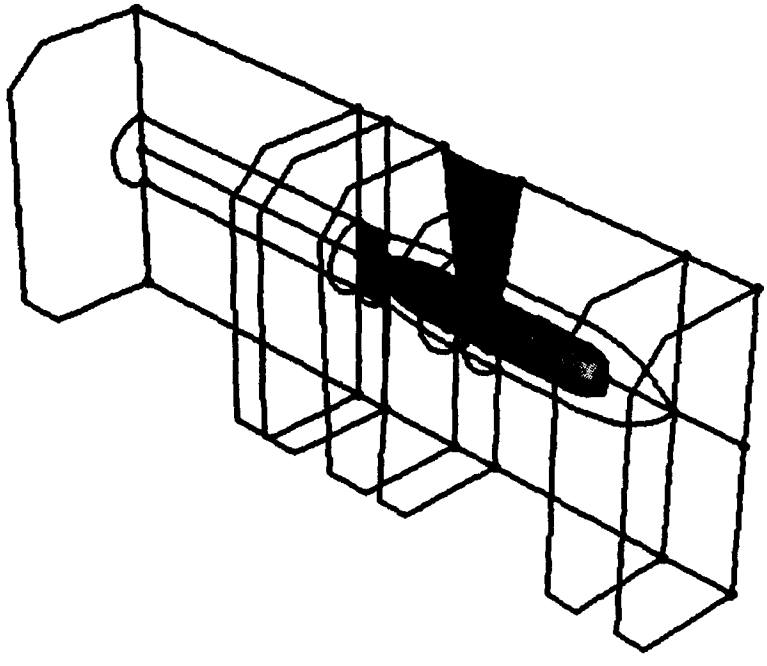

Fig. 4. Block structure for the 20-inch model in the LCC.

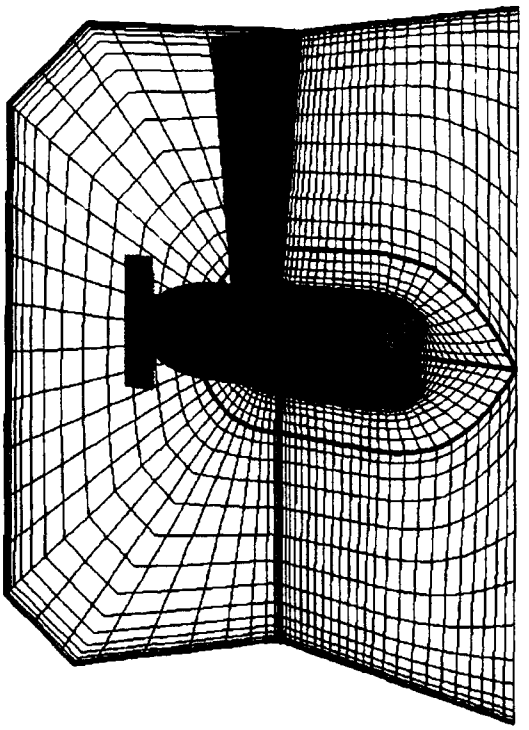

Fig. 5. Selected block faces for the 20-inch model in the LCC.

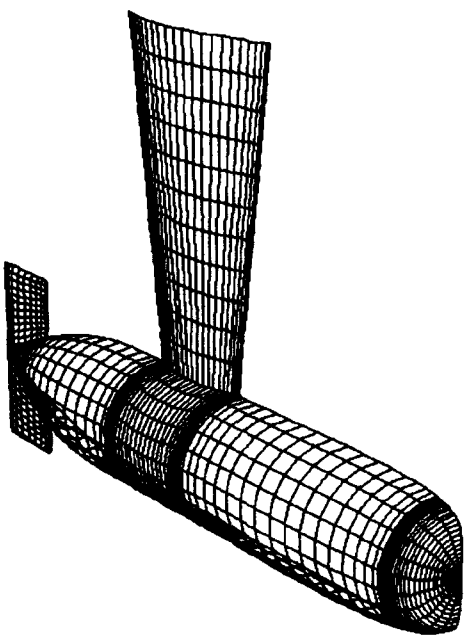

Fig. 6. Panel distribution used for inviscid flow calculations for the 20-inch model and strut.

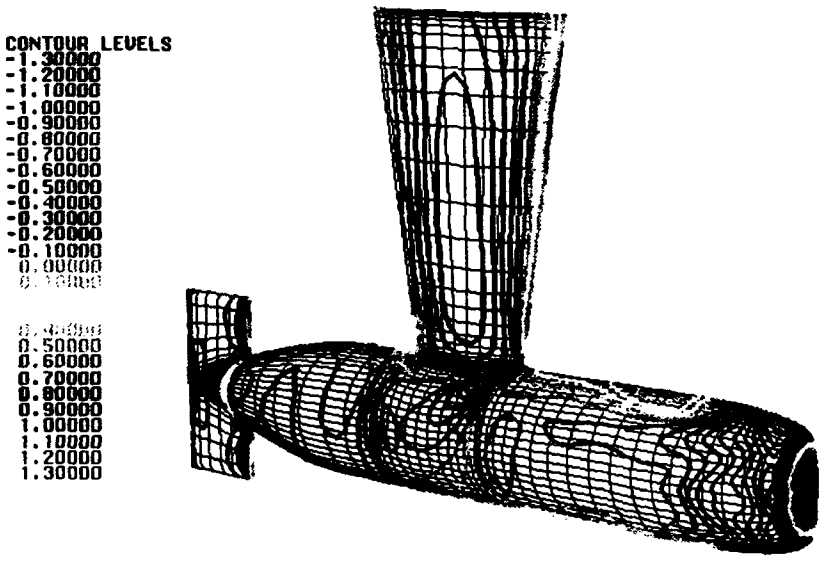

Fig. 7. Pressure coefficients on the 20-inch model and strut.

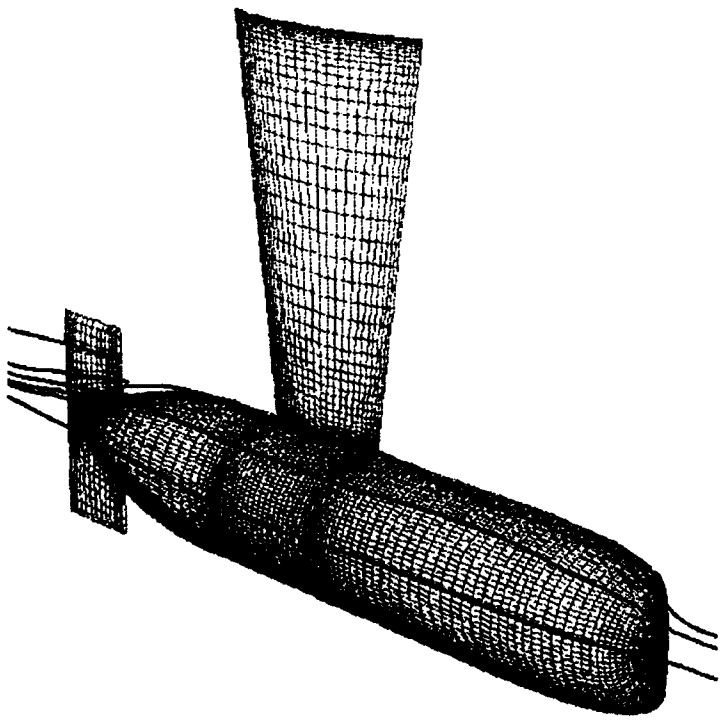

Fig. 8. Particle traces around the 20-inch model.

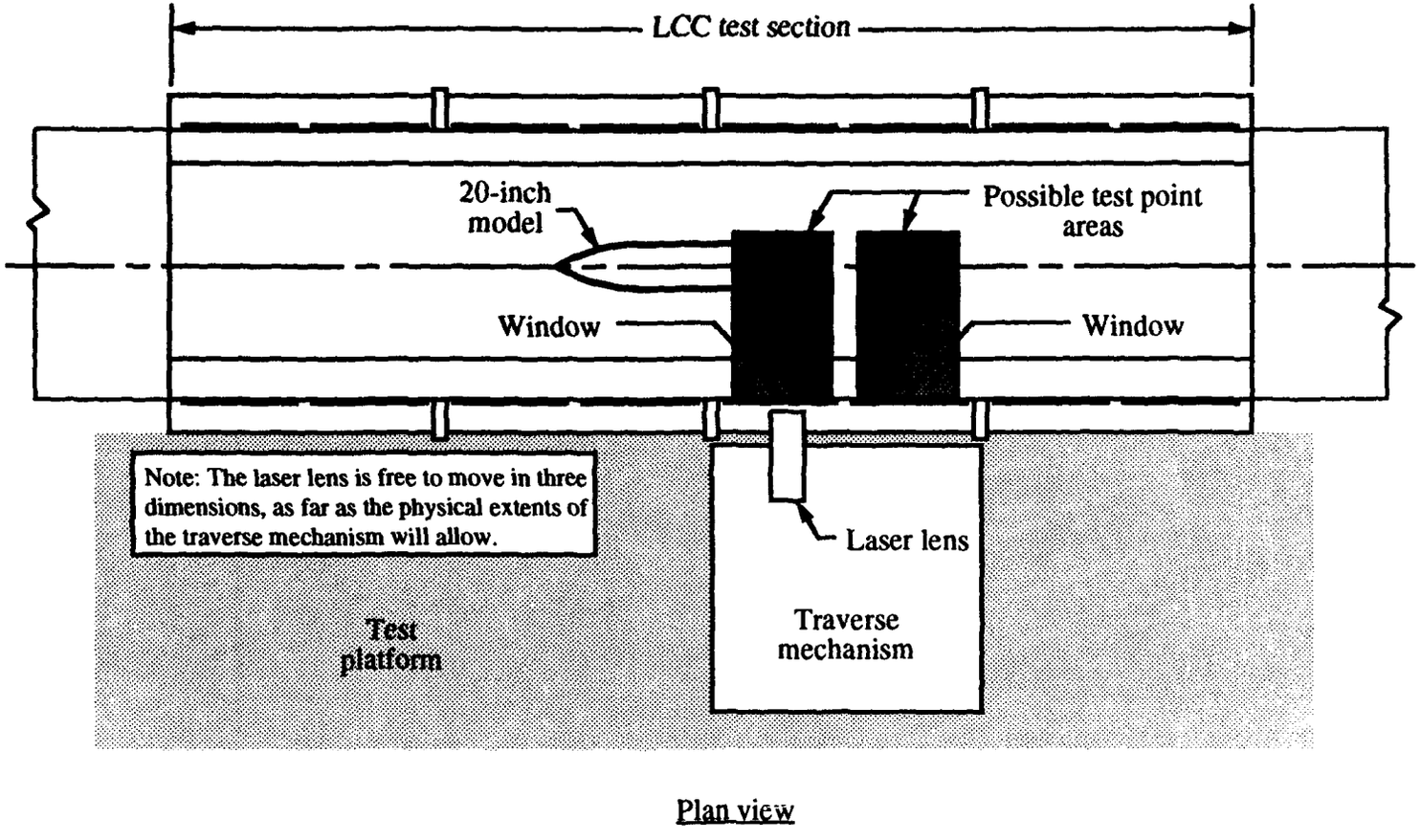

Fig. 9. Setup for LDV experiments with the 20-inch model.

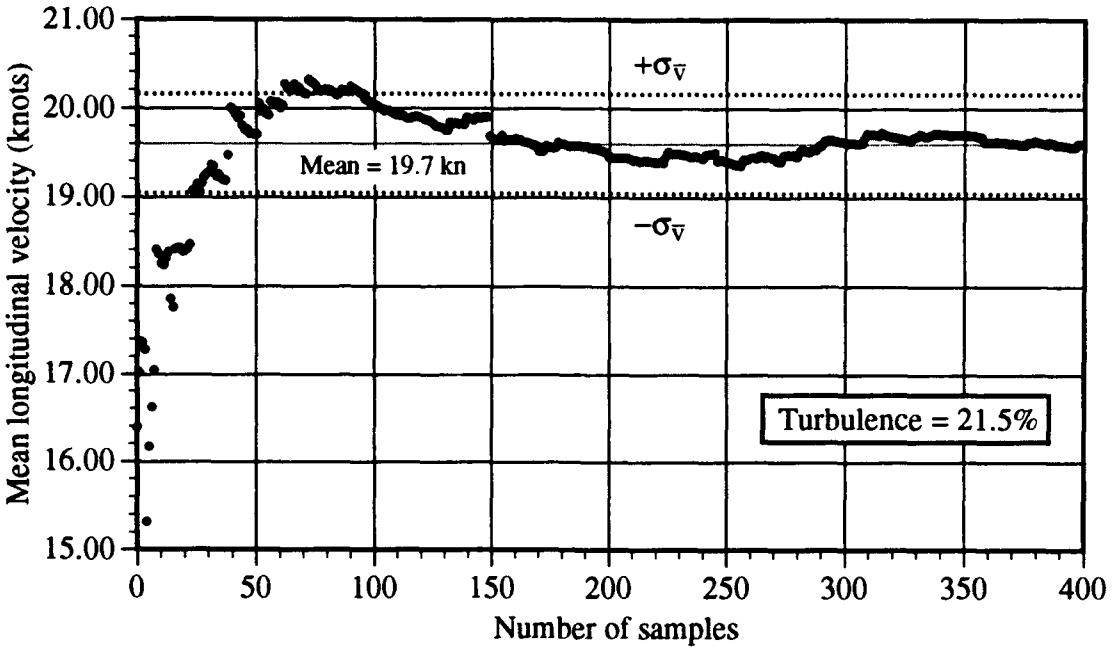

Fig. 10a. Samples taken near the tunnel wall.

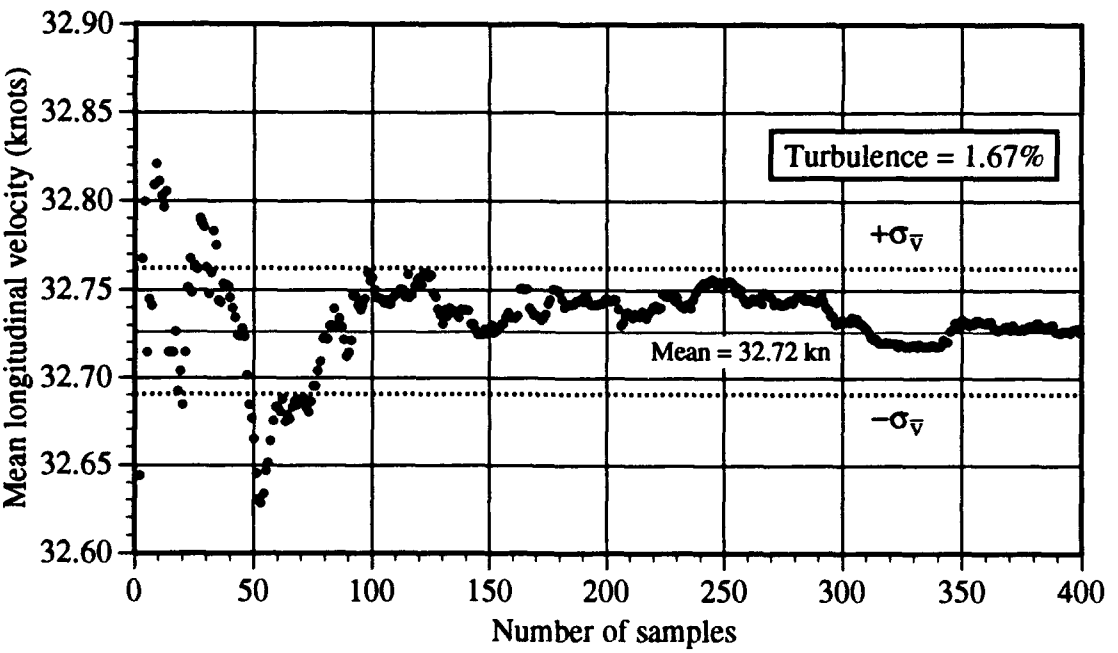

Fig. 10b. Samples taken at the upper edge of the model, near the model surface.

Fig. 10. Cumulative mean longitudinal velocities versus sample size.

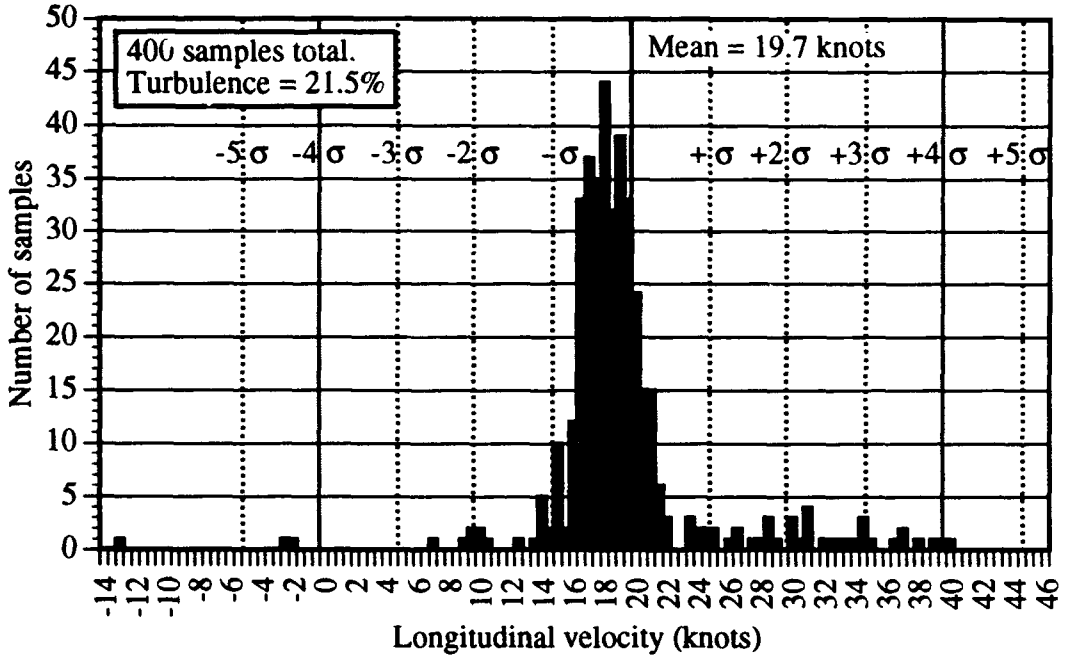

Fig. 11a. Samples taken near the tunnel wall.

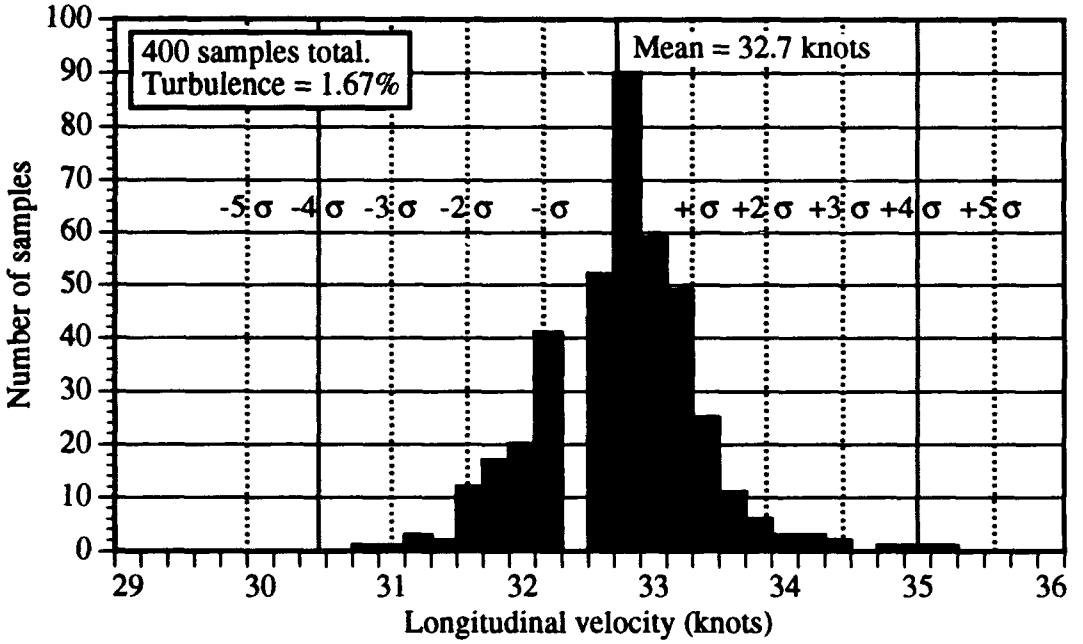

Fig. 11b. Samples taken at the upper edge of the model, near the model surface.

Fig. 11. Distribution of sample longitudinal velocities.

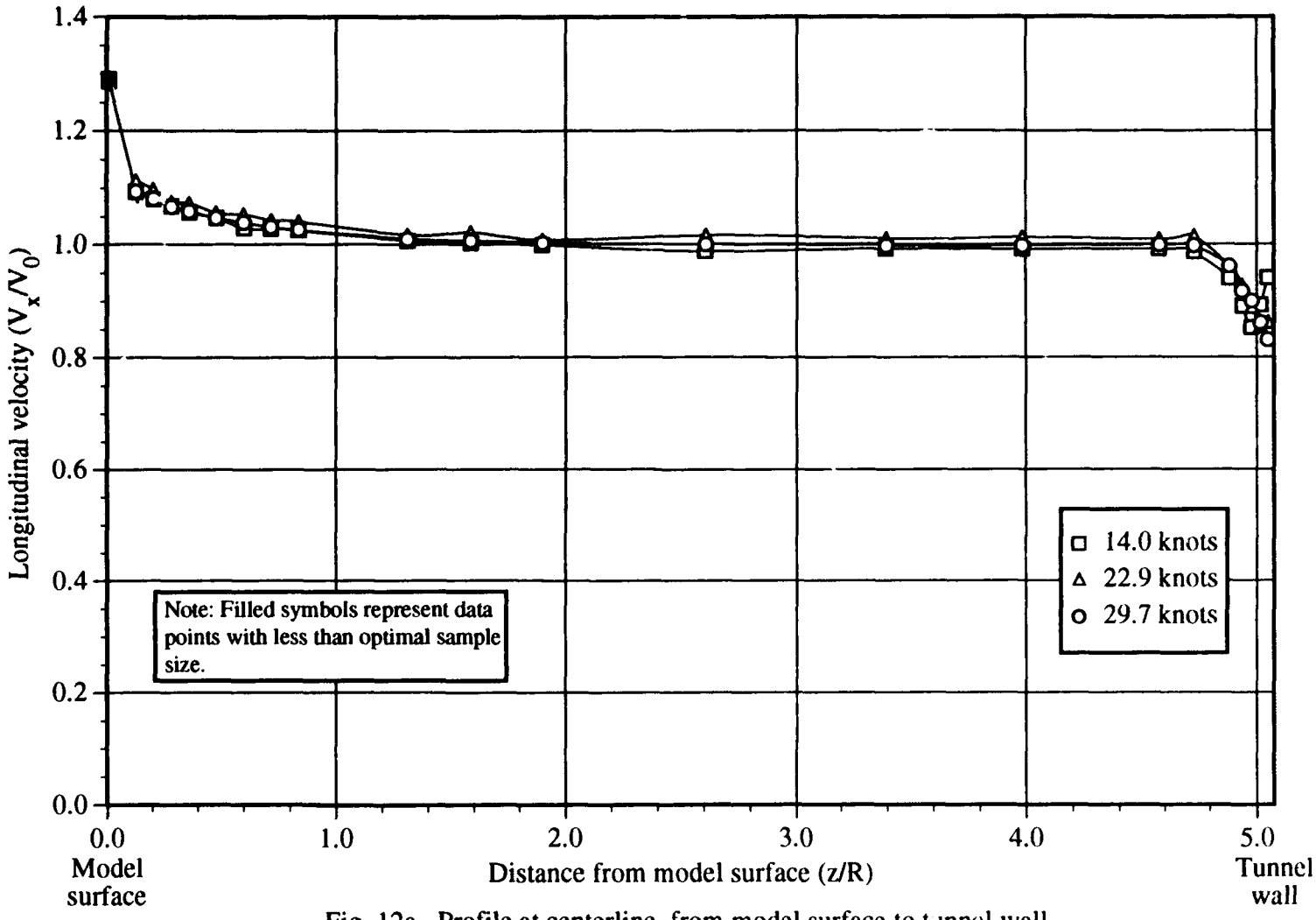

Fig. 12a. Profile at centerline, from model surface to tunnel wall.

Fig. 12. Experimental velocity profiles for the 20-inch model.

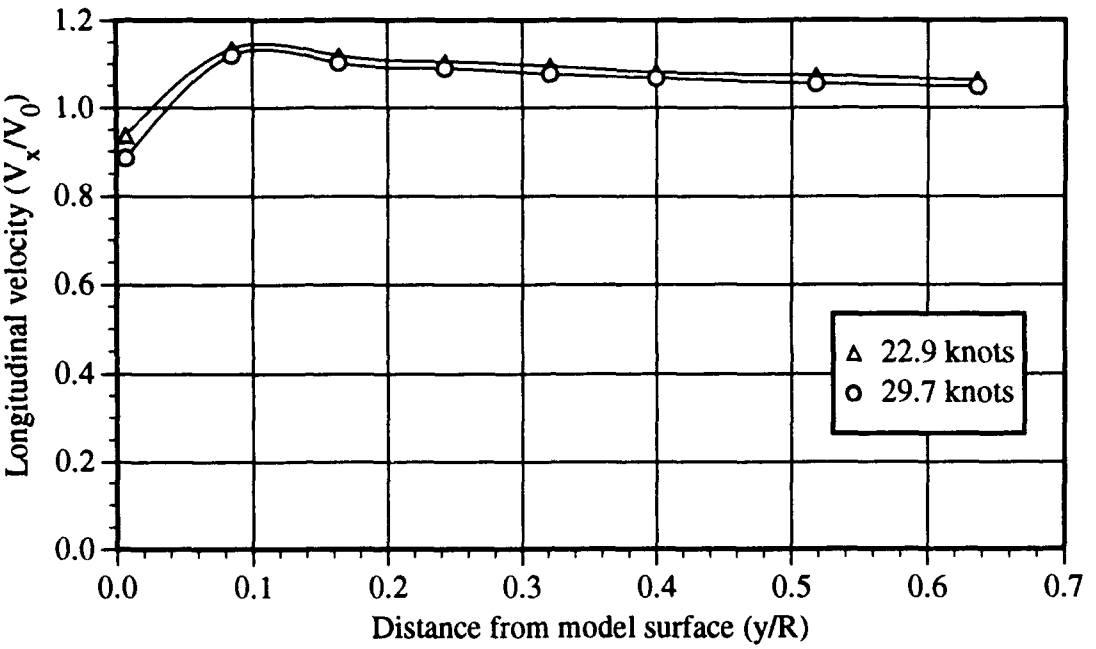

Fig. 12b. Profile around girth, at lower edge.

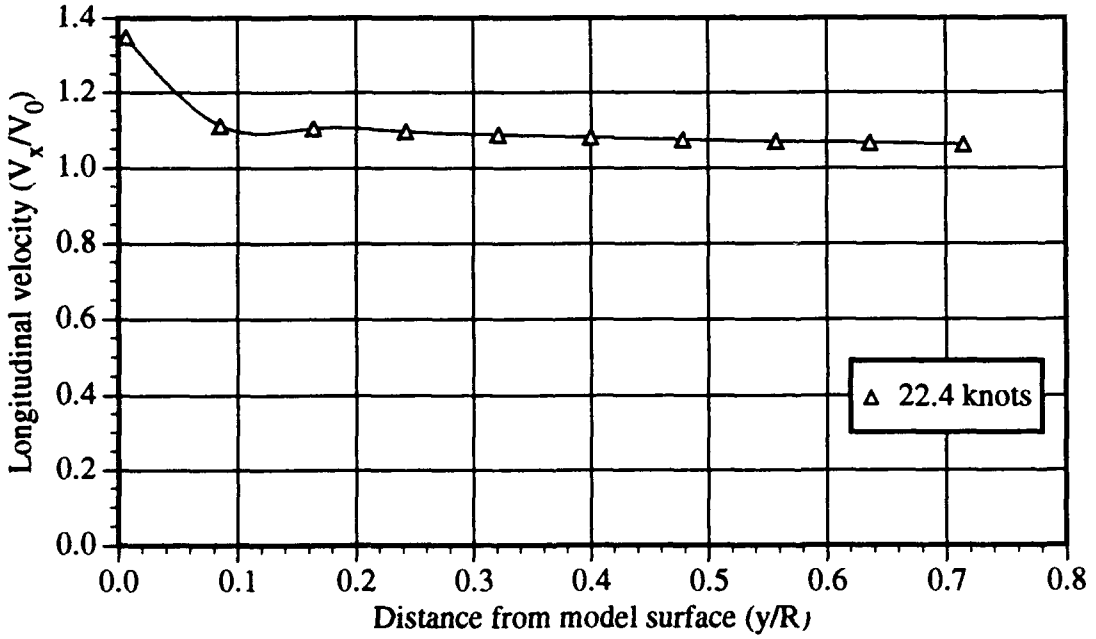

Fig. 12c. Profile along upper edge, 16 inches aft of stagnation point.

Fig. 12. (Continued.)

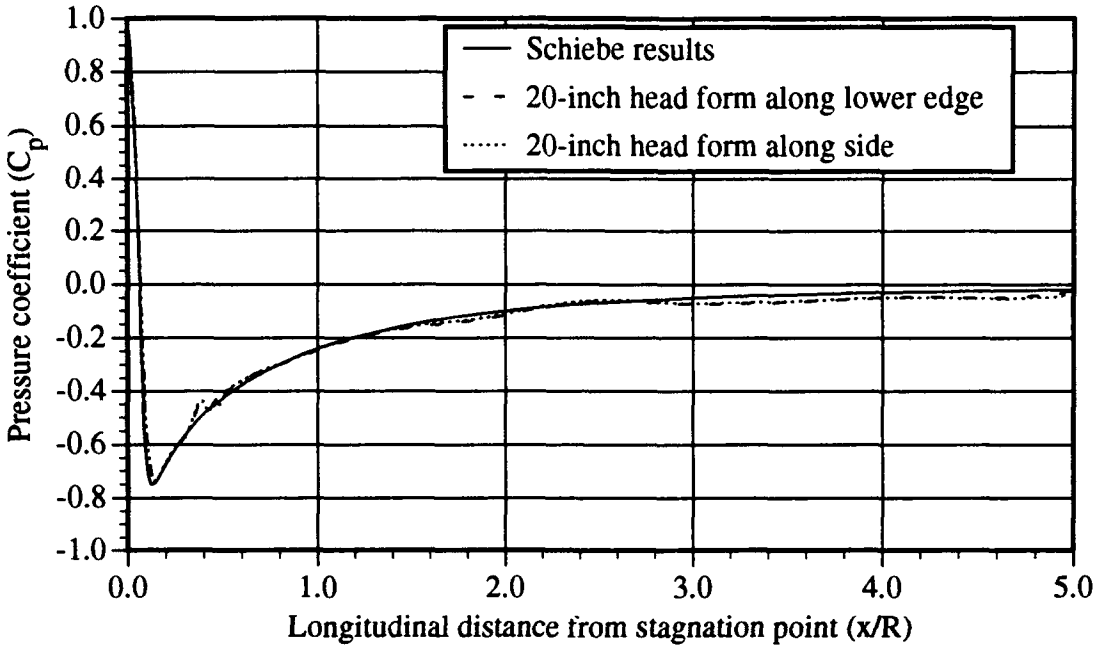

Fig. 13a. Pressure coefficients on the head form surface.

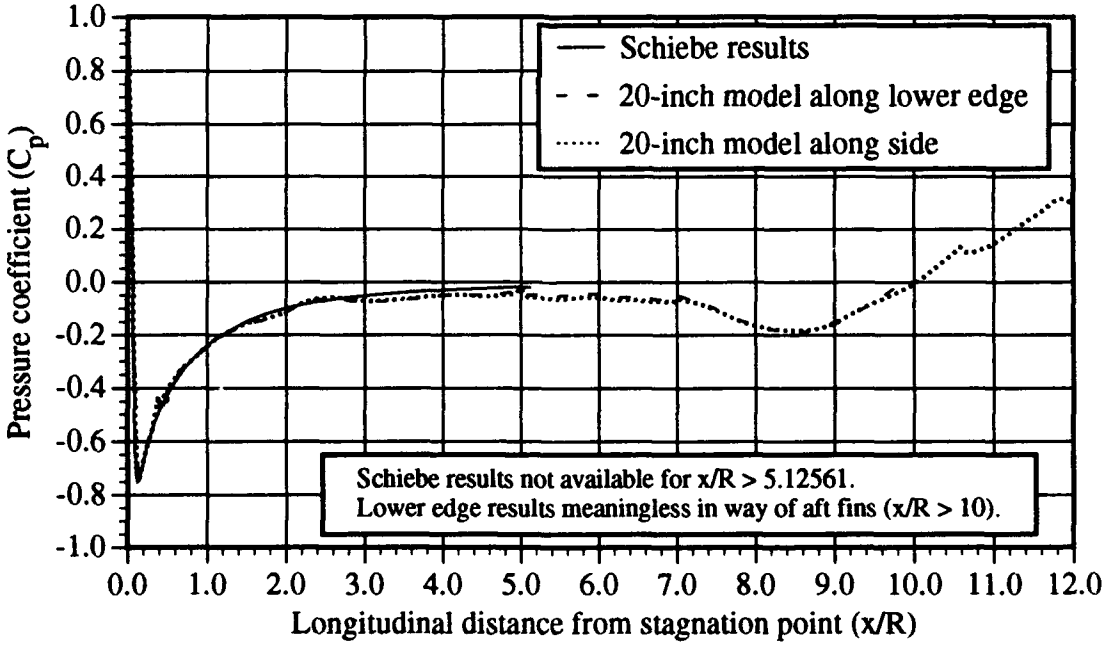

Fig. 13b. Pressure coefficients on the length of the model surface.

Fig. 13. Inviscid flow calculation results for the 20-inch model.

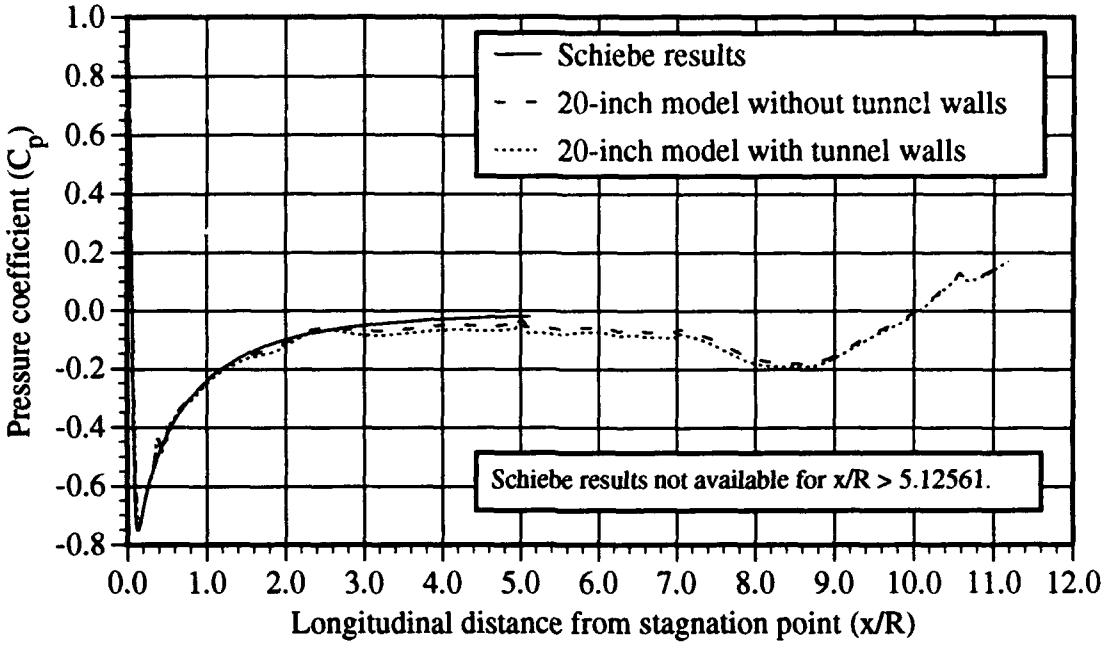

Fig. 14a. Pressure coefficients on the model surface.

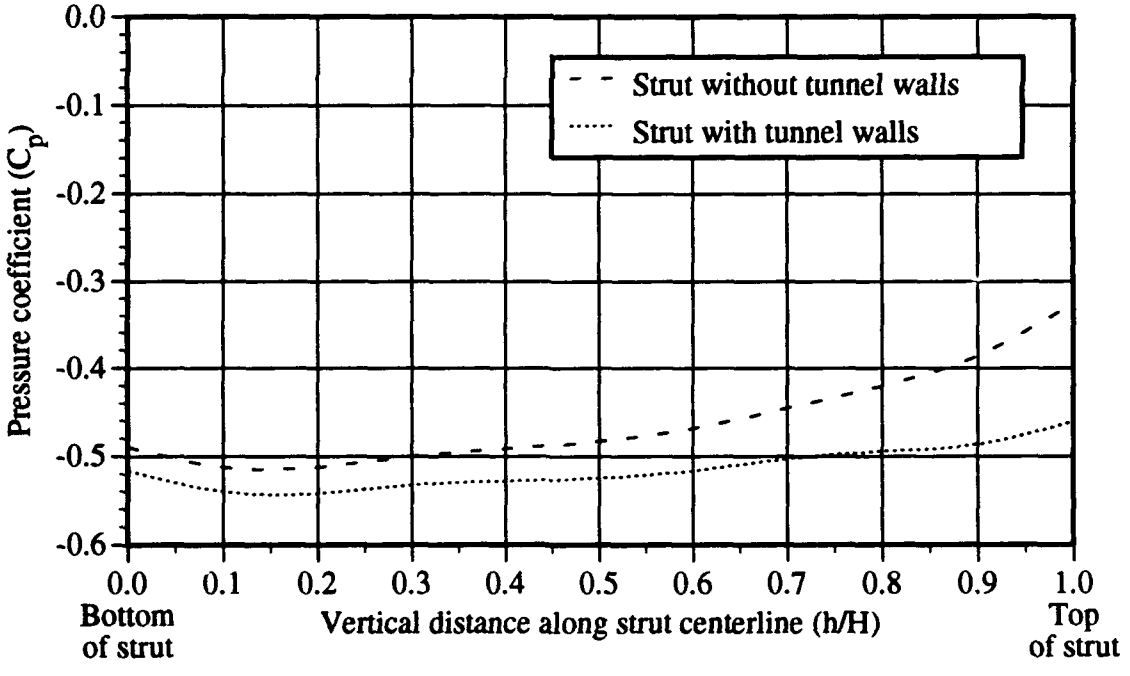

Fig. 14b. Pressure coefficients on the strut centerline.

Fig. 14. Inviscid flow calculation results for the 20-inch model with and without tunnel walls.

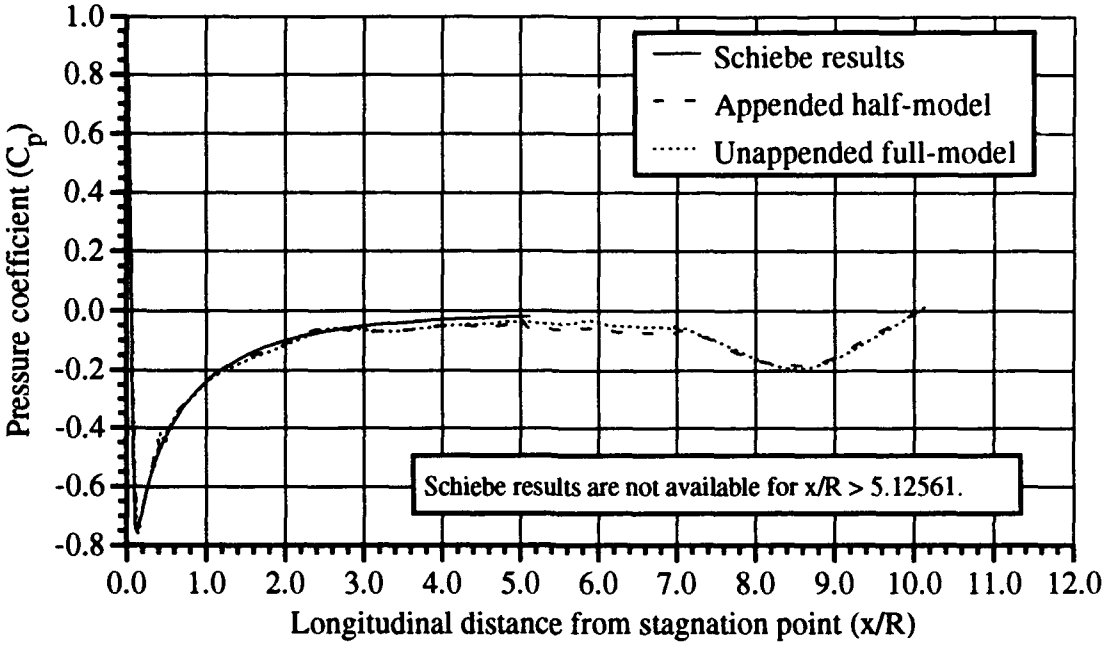

Fig. 15. Inviscid flow calculation results for the 20-inch half-model and full-model.

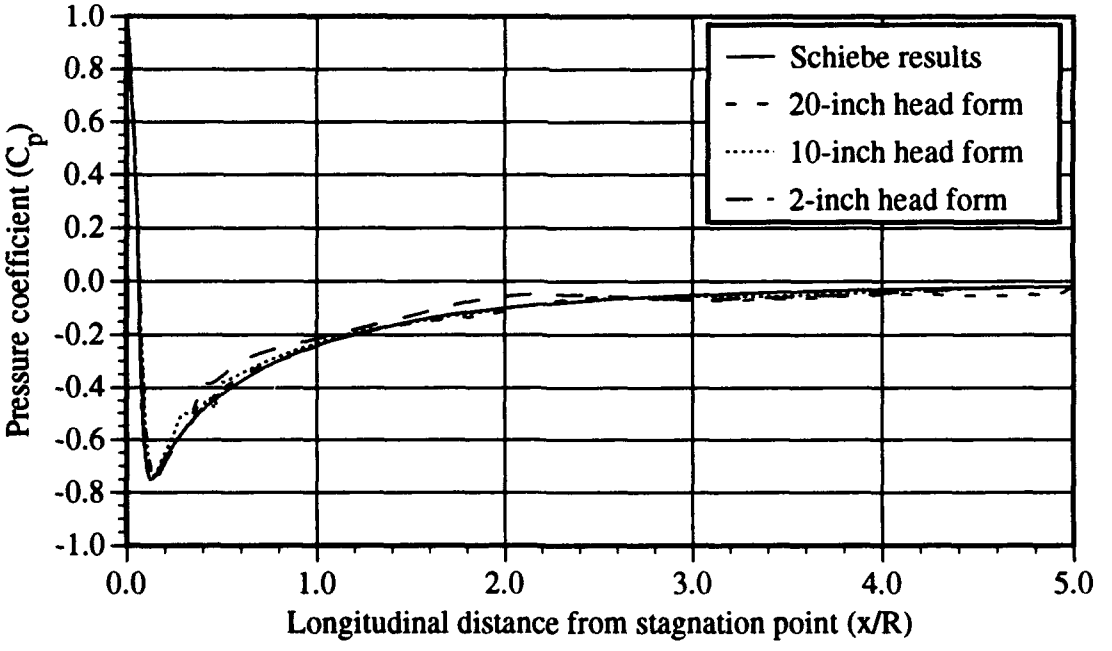

Fig. 16. Inviscid flow calculation results for three head forms.

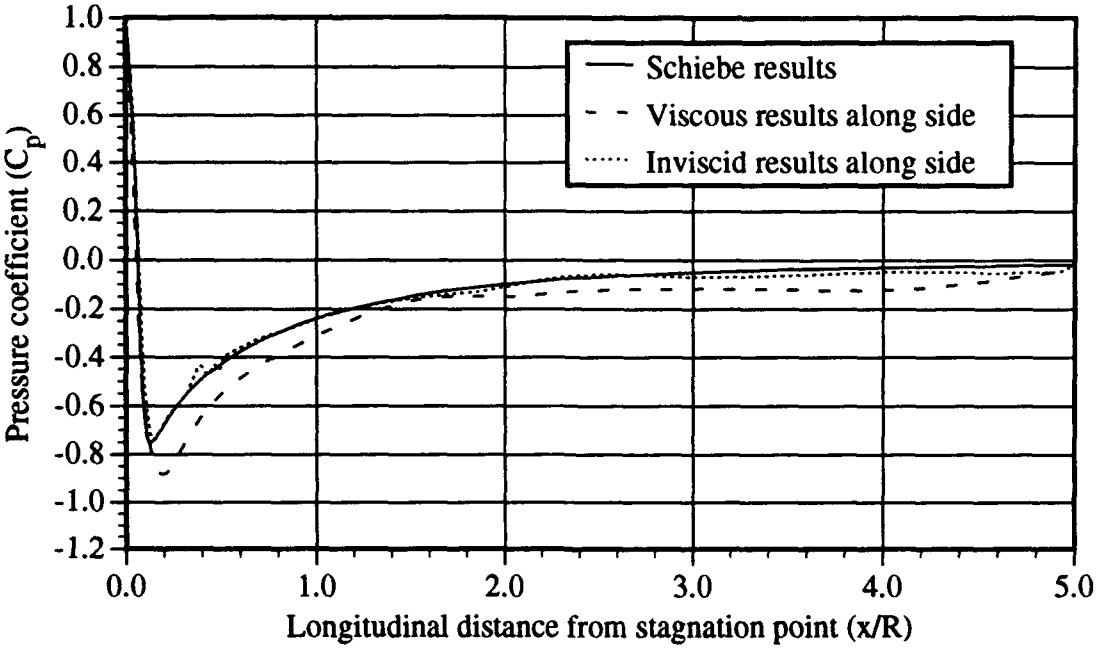

Fig. 17. Viscous and inviscid flow calculation results for the 20-inch model.

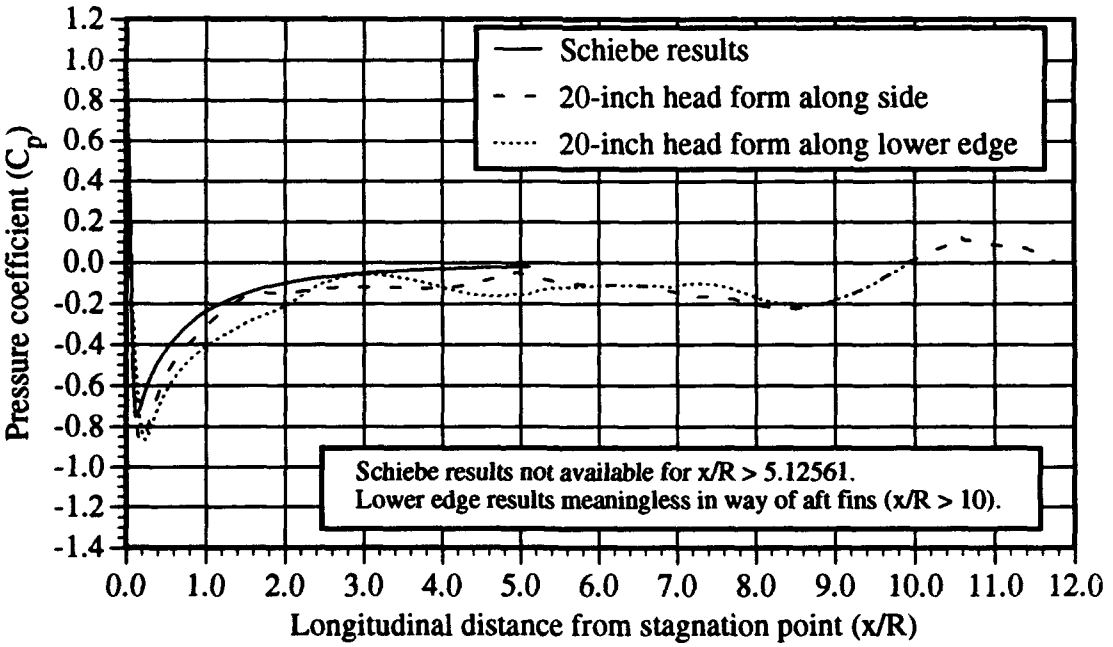

Fig. 18. Viscous flow calculation results for the 20-inch model.

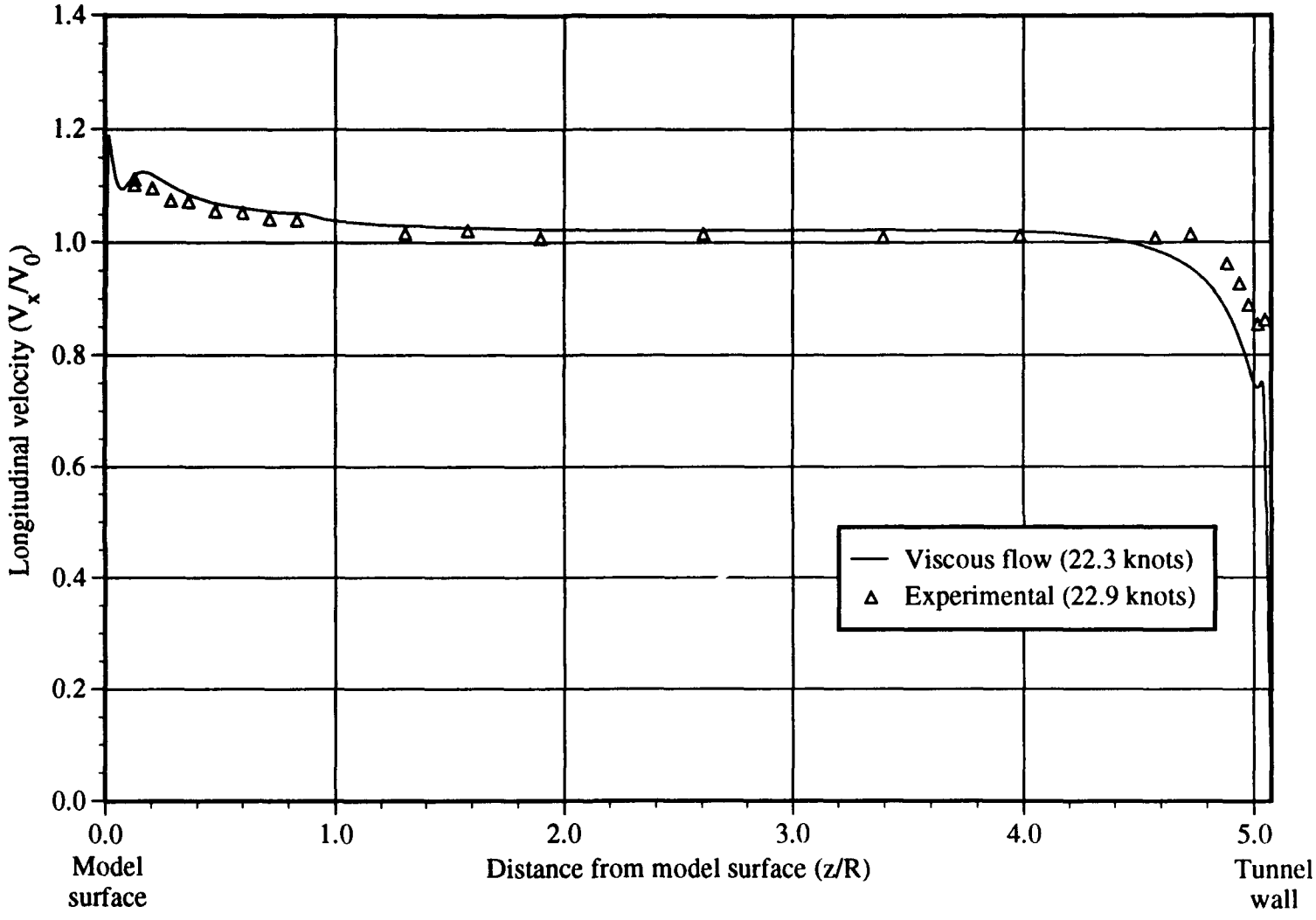

Fig. 19a. Profile at centerline, from model to tunnel wall.

Fig. 19. Viscous flow calculation results versus experimental data.

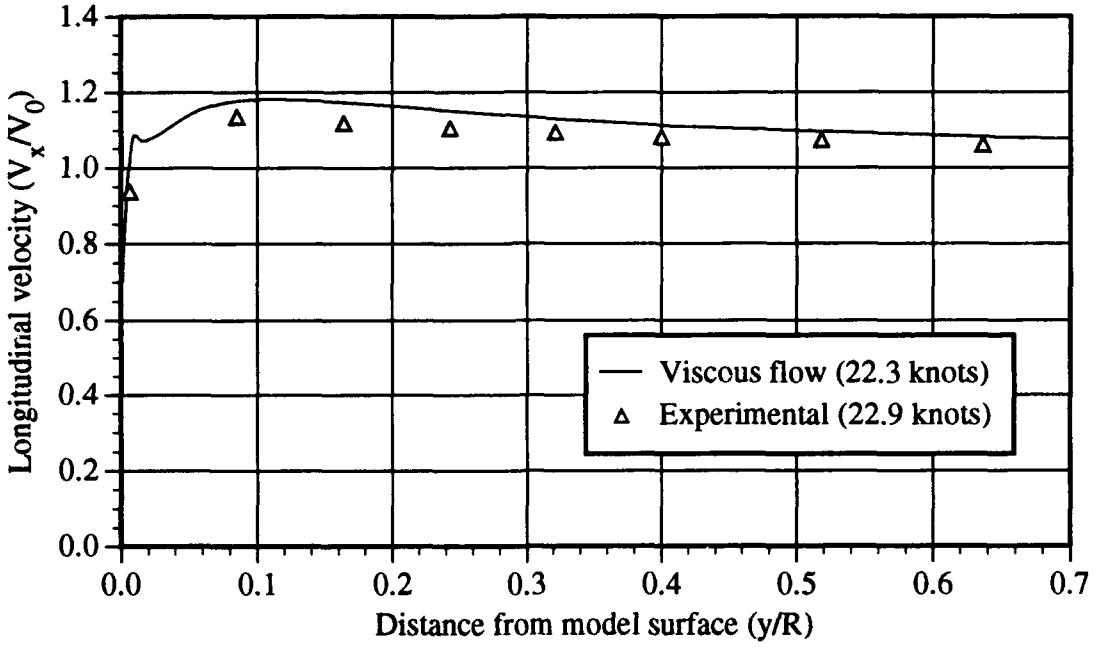

Fig. 19b. Profile around girth, at lower edge.

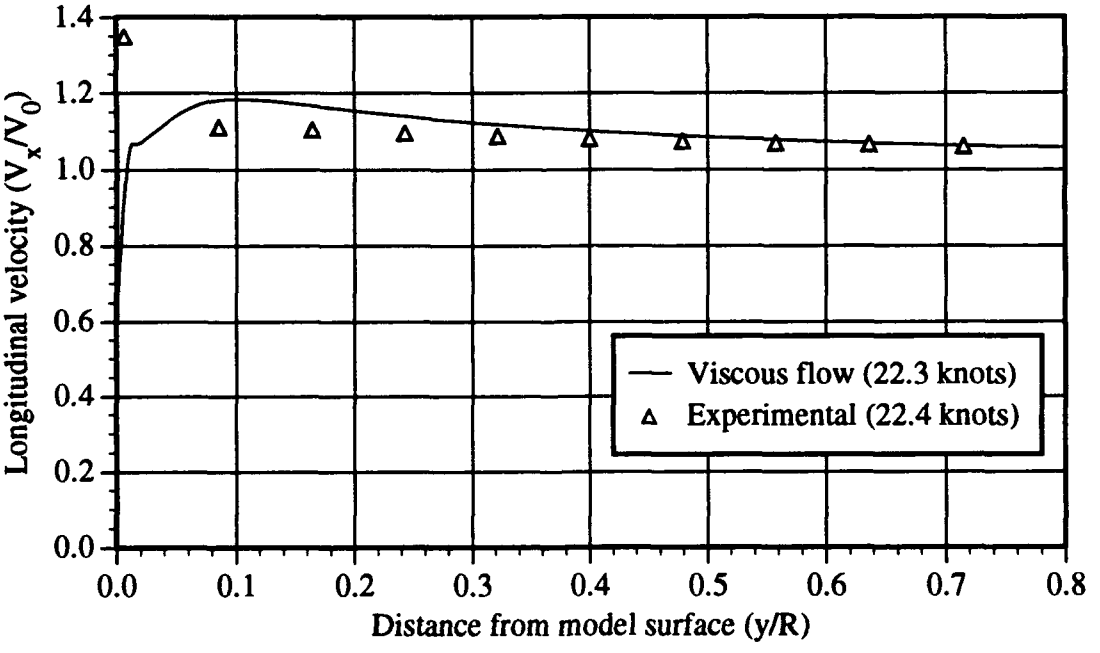

Fig. 19c. Profile along upper edge, 16 inches aft of stagnation point.

Fig. 19. (Continued).

THIS PAGE INTENTIONALLY LEFT BLANK.

APPENDIX A

DETAILED PROCEDURE FOR COMPUTATIONAL ANALYSIS

GEOMETRIC MODELLING

The first step of the computational analysis is to develop numerical models. Offsets are gathered from any available source: lines plans, model shop drawings, or electronic offsets. Typically, commercial software packages for personal computers, such as *MACSURF* or *FASTSHIP*, are used to generate the three-dimensional numerical surfaces representing the desired physical model, using conventional Bsplines or non-uniform, rational B-splines (NURBs). Conventional B-splines cannot precisely represent the shape of conic sections, but NURBs have this capability.

Sometimes, in a case such as the cavitation head forms, the models consist primarily of known geometrical shapes (e.g., nearly flat fins on a body of revolution and a tapered ogive strut). It is convenient to generate the models directly by writing a simple computer program to handle each specific geometry.

As the surfaces are defined, a grid is distributed over the surface. This step is handled by a program developed in-house called *REMESH*. In instances where the surfaces are defined directly, the surface is represented as a grid from the beginning, and this process is not an individual step. The intersections of the various surfaces are computed and the surfaces are trimmed to meet at the intersections without overlapping. Using another computer program (*NWIRE*, also developed in-house), shaded pictures are generated and visually inspected to ensure accurate surface generation.

Different types of numerical grids can be generated around the numerical models, for different methods of computational analysis, generally viscous flow or inviscid flow calculations. For the viscous flow analysis, a volume grid is developed, typically extending from the model surface to some outer boundary. For the inviscid flow analysis, a panelled surface is generated by redistributing the points on the surface grid.

VISCOUS FLOW CALCULATIONS

Grid Generation

Volume grids for viscous flow calculations can be developed using a computer package specifically developed for three-dimensional, multi-block grid generation. This package, called *GRIDGEN*, was developed by General Dynamics for the U.S. Air Force. Using *GRIDGEN*, the topology of the blocks and the connectivity of the blocks is defined. Tools in the *GRIDGEN* package allow for control of the grid size and distribution on each face of each block.

Once the face grids are defined, a program developed in-house called *TRANS3D* is used. *TRANS3D* determines the coordinates of the points on the interior of each block using a three-dimensional, algebraic, transfinite interpolation scheme. Essentially, the grids on the opposite faces of each block are projected through the interior of the block. By projecting through in three directions (three pairs of opposing faces on a six-sided block), points are located in space. These points outline cells, or three-dimensional volumes. The program checks each cell to ensure that the cells are oriented consistently with a right-handed coordinate system. Iterations of grid generation are made to achieve an acceptable three-dimensional volume grid with a relatively smooth, and properly oriented, grid distribution.

Solution Technique

The viscous flow calculations are made using a program called *ISFLOW*. The three-dimensional volume grid is developed for input to the program, and *ISFLOW* calculates a steady-state, incompressible flow solution using the three-dimensional Reynolds-averaged Navier-Stokes (RANS) equations. The three-dimensional velocity components are computed at each point in the grid through an iterative process for the steady-state solution. A more complete discussion of the program operation is given in Lin *et al.*[4]

A grid for an unappended surface ship might require about 400,000 points, versus over a million for a fully appended model. Grid points are typically concentrated in areas of high

curvature on the model, or in areas of rapidly changing flow conditions, such as near a stagnation point. The head form models therefore required about 600,000 grid points, due to the extremely rapid variation of flow characteristics near the forward end of the models (e.g., near the high curvature of the head form and near the stagnation point). A grid of this size requires about two-and-a-half minutes of computational time per iteration of the RANS equations on a powerful workstation, or about one minute on a super-computer. Typically, 2500 to 3000 iterations, or time-steps, are required before the program reaches a steady solution. A solution, therefore, requires anywhere from 50 to 125 hours of computer time to be calculated. Since the grid must be refined based on computational results, several incomplete runs of 500 or 1000 time-steps are generally made while the final grid is developed and refined. A single grid can require a total of 250 to 350 hours of computer time to reach a final solution.

INVISCID FLOW CALCULATIONS

Model Generation

Inviscid flow calculations typically require a panelled surface as input, which is generated by redistributing the points on the previously generated surface grid. Programs developed in-house called *REMESH* and *REPAN* allow control of the panel distribution, while ensuring that the panels conform to the surface shape. The panel distribution must be adjusted to concentrate more panels in areas of high curvature, radical change, or areas of special interest. At the same time, it is desirable to minimize the number of panels in order to minimize computation time. Rapid changes in panel size or aspect ratio can lead to poor computational results.

Solution Technique

The inviscid flow calculations can be made using several different computer programs. In this project, the calculations were made using a program called *VFLOW*. *VFLOW* does not account for a free surface, but a free-surface representation was not needed to examine the flow

in a closed tunnel such as the LCC.

A panelled surface is supplied as input to the program, and the program then distributes doublet and source singularities over the surface. *VFLOW* assumes incompressible flow. Local velocity in three components and pressure coefficient are calculated for each panel. As indicated by the name, inviscid flow calculations do not account for viscous effects, such as turbulence and separation.

An inviscid model typically has 1500 to 2500 panels, versus hundreds of thousands to over a million grid points for a viscous grid. The solution time is correspondingly quicker. An inviscid flow solution can take anywhere from 2 to 5 minutes of computational time. Even multiple iterations while refining the model do not involve much computer time.

PRESENTATION OF RESULTS

The output produced by *ISFLOW* includes a flow solution file that contains pressure and velocities in three components for each point. This solution file and the grid coordinate file were used to display the results in various graphical formats. A program called *PLOT3D*, developed by NASA Ames Research Center, is often used to produce three-dimensional plots of geometry, grids, and computational results as streamlines, vectors, contours, etc.

PLOT3D was developed for compressible flow. Pressure and velocity are converted to density, stagnation energy, and momentum values. *PLOT3D* can then be used to represent these values as streamlines, vectors, contours, etc. of various functions. The *PLOT3D* user's manual[5] contains a complete list of available functions.

No programs were available specifically for viewing the inviscid flow calculation results. However, *PLOT3D* is versatile enough to accept a modified input file for basic plotting. Plotting was limited to the specifically generated output from *VFLOW*. No plots could be made where no information was present (e.g., anywhere off the model or strut surface.)

In addition, the results can be graphed in two-dimensional formats using various

commercially available graphing/plotting packages.

APPENDIX B

EXPERIMENTAL RESULTS FOR THE 20-INCH HEAD FORM IN THE LCC

Table B-1. Experimental data.

Table B-1a. Profile along lower edge, forward of $C_{p,min}$, 22.8 knots.

Profile along lower edge, forward of $C_{p,min}$.							Tunnel speed:	22.8	knots
							Tunnel pressure:	12.7	psia
Point	X (in.)	Y (in.)	Z (in.)	Distance from surface (in.)	Velocity (knots)	Velocity (V_x/V_0)	Turbulence (%)	Number of points	/ outliers
Surface	1.396	6.858	0.000						
1	1.024	7.230	0.000	0.527	21.70	0.952	1.59	500	/ 2
2	0.827	7.427	0.000	0.805	20.53	0.900	2.01	500	/ 1
3	0.630	7.624	0.000	1.084	20.12	0.883	1.86	500	/ 1
4	0.433	7.821	0.000	1.362	19.92	0.874	1.79	500	/ 2
5	0.236	8.018	0.000	1.641	19.86	0.871	1.42	500	/ 5
6	0.039	8.215	0.000	1.919	19.88	0.872	1.36	47	/ 0

Table B-1b. Profile along lower edge, 8 inches aft of stagnation point, 22.8 knots.

Profile along lower edge, 8 inches aft of stagnation point.							Tunnel speed:	22.8	knots
							Tunnel pressure:	12.7	psia
Point	X (in.)	Y (in.)	Z (in.)	Distance from surface (in.)	Velocity (knots)	Velocity (V_x/V_0)	Turbulence (%)	Number of points	/ outliers
Surface	7.638	9.252	0.000						
1	7.638	9.317	0.000	0.065	22.11	0.970	8.46	500	/ 0
2	7.638	10.104	0.000	0.852	26.03	1.142	2.14	436	/ 0
3	7.638	10.892	0.000	1.640	25.49	1.118	2.25	449	/ 1
4	7.638	11.679	0.000	2.427	25.01	1.097	2.12	463	/ 1
5	7.638	12.467	0.000	3.214	24.78	1.087	2.13	462	/ 1
6	7.638	13.254	0.000	4.002	24.60	1.079	2.12	450	/ 1
7	7.638	14.435	0.000	5.183	24.36	1.068	2.09	450	/ 2
8	7.638	15.616	0.000	6.364	24.22	1.062	2.08	448	/ 1

Table B-1. (Continued.)

Table B-1c. Profile forward of stagnation point, 29.7 knots.

Profile forward of stagnation point.							Tunnel speed: 29.7 knots Tunnel pressure: 17.0 psia	
Point	X (in.)	Y (in.)	Z (in.)	Distance from surface (in.)	Velocity (knots)	Velocity (V_x/V_0)	Turbulence (%)	Number of points / outliers
Surface	0.000	-0.014	0.000					
1	-17.323	-0.014	0.000	17.323	27.60	0.929	1.60	400 / 2
2	-18.110	-0.014	0.000	18.110	27.76	0.935	1.74	400 / 0
3	-18.898	-0.014	0.000	18.898	27.92	0.940	1.66	400 / 0
4	-19.685	-0.014	0.000	19.685	27.97	0.942	1.63	400 / 1
5	-20.472	-0.014	0.000	20.472	28.01	0.943	1.20	42 / 0
6	-21.260	-0.014	0.000	21.260	28.21	0.950	1.50	154 / 0

Table B-1. (Continued.)

Table B-1d. Profile around girth, at upper edge, 22.9 knots.

Profile around girth, at upper edge.							Tunnel speed: 22.9 knots Tunnel pressure: 17.1 psia		
Point	X (in.)	Y (in.)	Z (in.)	Distance from surface (in.)	Velocity (knots)	Velocity (V_x/V_0)	Turbulence (%)	Number of points	/ outliers
Surface	7.638	-9.252	0.000						
1	7.638	-9.325	0.000	0.073	21.11	0.922	9.86	400	/ 0
2	7.638	-10.112	0.000	0.860	25.40	1.109	1.98	400	/ 0
3	7.638	-10.900	0.000	1.647	25.08	1.095	2.19	400	/ 1
4	7.638	-11.687	0.000	2.435	24.82	1.084	2.13	400	/ 0
5	7.638	-12.474	0.000	3.222	24.54	1.072	2.01	400	/ 0
6	7.638	-13.262	0.000	4.010	24.37	1.064	1.92	400	/ 0
7	7.638	-14.443	0.000	5.191	24.15	1.055	2.29	400	/ 0
8	7.638	-15.624	0.000	6.372	24.08	1.052	2.39	400	/ 0
9	7.638	-16.805	0.000	7.553	23.86	1.042	2.32	400	/ 2
10	7.638	-17.986	0.000	8.734	23.78	1.038	2.27	400	/ 1

Table B-1e. Profile around girth, at upper edge, 29.7 knots.

Profile around girth, at upper edge.							Tunnel speed: 29.7 knots Tunnel pressure: 17.0 psia		
Point	X (in.)	Y (in.)	Z (in.)	Distance from surface (in.)	Velocity (knots)	Velocity (V_x/V_0)	Turbulence (%)	Number of points	/ outliers
Surface	7.638	-9.252	0.000						
1	7.638	-9.325	0.000	0.073	28.85	0.971	7.61	400	/ 0
2*	7.638	-10.112	0.000	0.860	32.72	1.102	1.67	400	/ 2
3	7.638	-10.900	0.000	1.647	32.23	1.085	1.75	400	/ 0
4	7.638	-11.687	0.000	2.435	31.82	1.071	1.57	400	/ 0
5	7.638	-12.474	0.000	3.222	31.46	1.059	1.64	400	/ 1
6	7.638	-13.262	0.000	4.010	31.24	1.052	1.52	400	/ 3
7	7.638	-14.443	0.000	5.191	30.92	1.041	1.65	400	/ 0
8	7.638	-15.624	0.000	6.372	30.68	1.033	1.71	400	/ 0
9	7.638	-16.805	0.000	7.553	30.48	1.026	1.77	400	/ 0
10	7.638	-17.986	0.000	8.734	30.29	1.020	1.83	400	/ 0

* This point is the low turbulence data point shown in Figures 9b and 10b.

Table B-1. (Continued.)

Table B-1f. Profile around girth, at 45° above centerline, 22.8 knots.

Profile around girth, at 45° above centerline.							Tunnel speed: 22.8 knots Tunnel pressure: 17.1 psia	
Point	X (in.)	Y (in.)	Z (in.)	Distance from surface (in.)	Velocity (knots)	Velocity (V_x/V_0)	Turbulence (%)	Number of points / outliers
Surface	7.638	-5.401	5.401					
1	7.638	-6.470	7.094	2.003	23.66	1.038	14.97	8 / 0
2	7.638	-7.061	7.685	2.824	25.21	1.106	2.23	400 / 2
3	7.638	-7.652	8.276	3.651	24.92	1.093	2.36	400 / 0
4	7.638	-8.242	8.866	4.481	24.61	1.079	2.52	400 / 0
5	7.638	-8.833	9.457	5.313	24.35	1.068	2.65	400 / 1
6	7.638	-9.423	10.047	6.146	24.11	1.057	2.36	400 / 1
7	7.638	-10.211	10.835	7.257	23.93	1.050	2.60	400 / 1
8	7.638	-11.195	11.819	8.647	23.72	1.040	2.71	400 / 0
9	7.638	-11.982	12.606	9.759	23.62	1.036	2.63	400 / 0
10	7.638	-12.770	13.394	10.872	23.45	1.028	2.58	400 / 1

Table B-1g. Profile around girth, at 45° above centerline, 22.8 knots.

Profile around girth, at 45° above centerline.							Tunnel speed: 29.7 knots Tunnel pressure: 17.0 psia	
Point	X (in.)	Y (in.)	Z (in.)	Distance from surface (in.)	Velocity (knots)	Velocity (V_x/V_0)	Turbulence (%)	Number of points / outliers
Surface	7.638	-5.401	5.401					
1	7.638	-6.470	7.094	2.003	32.38	1.090	10.38	204 / 5
2	7.638	-7.061	7.685	2.824	32.44	1.092	1.53	400 / 0
3	7.638	-7.652	8.276	3.651	31.93	1.075	1.67	400 / 1
4	7.638	-8.242	8.866	4.481	31.56	1.063	1.62	400 / 1
5	7.638	-8.833	9.457	5.313	31.32	1.055	1.69	400 / 1
6	7.638	-9.423	10.047	6.146	31.08	1.047	1.83	400 / 0
7	7.638	-10.211	10.835	7.257	30.85	1.039	1.71	400 / 2
8	7.638	-11.195	11.819	8.647	30.62	1.031	1.81	400 / 1
9	7.638	-11.982	12.606	9.759	30.38	1.023	1.79	400 / 0
10	7.638	-12.770	13.394	10.872	30.28	1.020	1.71	400 / 0

Table B-1. (Continued.)

Table B-1h. Profile around girth, at centerline, 22.9 knots.

Profile around girth, at centerline.							Tunnel speed:	22.9	knots
							Tunnel pressure:	20.1	psia
Point	X (in.)	Y (in.)	Z (in.)	Distance from surface (in.)	Velocity (knots)	Velocity (V_x/V_0)	Turbulence (%)	Number of points /	outliers
Surface	7.638	-0.014	9.252						
1	7.638	-0.014	9.339	0.086	25.82	1.127	14.17	400 /	13
2	7.638	-0.014	9.732	0.480	25.63	1.119	2.00	400 /	1
3	7.638	-0.014	10.520	1.267	25.31	1.105	2.36	400 /	0
4	7.638	-0.014	11.307	2.055	24.94	1.089	2.34	400 /	0
5	7.638	-0.014	12.094	2.842	24.72	1.079	2.50	400 /	0
6	7.638	-0.014	12.882	3.630	24.50	1.070	2.26	400 /	1
7	7.638	-0.014	14.063	4.811	24.15	1.054	2.52	400 /	1
8	7.638	-0.014	15.244	5.992	23.92	1.044	2.37	400 /	1
9	7.638	-0.014	16.425	7.173	23.77	1.038	2.58	400 /	0
10	7.638	-0.014	17.606	8.354	23.64	1.032	2.65	400 /	0

Table B-1i. Profile around girth, at centerline, 29.7 knots.

Profile around girth, at centerline.							Tunnel speed:	29.7	knots
							Tunnel pressure:	17.0	psia
Point	X (in.)	Y (in.)	Z (in.)	Distance from surface (in.)	Velocity (knots)	Velocity (V_x/V_0)	Turbulence (%)	Number of points /	outliers
Surface	7.638	-0.014	9.252						
1	7.638	-0.014	9.339	0.086	32.77	1.103	9.13	400 /	9
2	7.638	-0.014	9.732	0.480	33.02	1.112	1.77	400 /	0
3	7.638	-0.014	10.520	1.267	32.52	1.095	1.59	400 /	1
4	7.638	-0.014	11.307	2.055	32.10	1.081	1.64	400 /	2
5	7.638	-0.014	12.094	2.842	31.72	1.068	1.56	400 /	1
6	7.638	-0.014	12.882	3.630	31.41	1.058	1.73	400 /	0
7	7.638	-0.014	14.063	4.811	31.09	1.047	1.54	400 /	0
8	7.638	-0.014	15.244	5.992	30.84	1.038	1.59	400 /	0
9	7.638	-0.014	16.425	7.173	30.68	1.033	1.72	400 /	1
10	7.638	-0.014	17.606	8.354	30.49	1.026	1.73	400 /	1

Table B-1. (Continued.)

Table B-1j. Profile around girth, at 45° below centerline, 22.9 knots.

Profile around girth, at 45° below centerline.							Tunnel speed: 22.9 knots Tunnel pressure: 20.1 psia		
Point	X (in.)	Y (in.)	Z (in.)	Distance from surface (in.)	Velocity (knots)	Velocity (V_x/V_0)	Turbulence (%)	Number of points	/ outliers
Surface	7.638	5.401	5.401						
1	7.638	6.443	7.094	1.989	25.94	1.133	2.31	400	/ 1
2	7.638	7.033	7.685	2.808	25.57	1.116	2.22	400	/ 0
3	7.638	7.624	8.276	3.634	25.19	1.100	2.16	400	/ 0
4	7.638	8.215	8.866	4.464	24.99	1.091	2.35	400	/ 1
5	7.638	8.805	9.457	5.295	24.68	1.078	2.16	400	/ 0
6	7.638	9.396	10.047	6.128	24.49	1.070	2.36	400	/ 0
7	7.638	10.183	10.835	7.239	24.31	1.062	2.33	400	/ 0
8	7.638	11.167	11.819	8.628	24.11	1.053	2.47	400	/ 0
9	7.638	11.955	12.606	9.740	23.97	1.047	2.34	400	/ 2
10	7.638	12.742	13.394	10.853	23.86	1.042	2.18	400	/ 1

Table B-1k. Profile around girth, at 45° below centerline, 29.7 knots.

Profile around girth, at 45° below centerline.							Tunnel speed: 29.7 knots Tunnel pressure: 17.0 psia		
Point	X (in.)	Y (in.)	Z (in.)	Distance from surface (in.)	Velocity (knots)	Velocity (V_x/V_0)	Turbulence (%)	Number of points	/ outliers
Surface	7.638	5.401	5.401						
1	7.638	6.443	7.094	1.989	33.39	1.124	1.67	400	/ 0
2	7.638	7.033	7.685	2.808	32.95	1.110	1.66	400	/ 0
3	7.638	7.624	8.276	3.634	32.41	1.091	1.57	400	/ 1
4	7.638	8.215	8.866	4.464	32.01	1.078	1.75	400	/ 0
5	7.638	8.805	9.457	5.295	31.72	1.068	1.70	400	/ 0
6	7.638	9.396	10.047	6.128	31.38	1.057	1.75	400	/ 1
7	7.638	10.183	10.835	7.239	31.09	1.047	1.73	400	/ 0
8	7.638	11.167	11.819	8.628	30.80	1.037	1.66	400	/ 0
9	7.638	11.955	12.606	9.740	30.61	1.031	1.57	400	/ 0
10	7.638	12.742	13.394	10.853	30.55	1.028	1.69	400	/ 2

Table B-1. (Continued.)

Table B-11. Profile around girth, at lower edge, 22.9 knots.

Profile around girth, at lower edge.*							Tunnel speed:	22.9	knots
							Tunnel pressure:	20.1	psia
Point	X (in.)	Y (in.)	Z (in.)	Distance from surface (in.)	Velocity (knots)	Velocity (V_x/V_0)	Turbulence (%)	Number of points / outliers	
Surface	7.638	9.252	0.000						
1	7.638	9.317	0.000	0.065	21.47	0.938	9.63	400 /	0
2	7.638	10.104	0.000	0.852	25.99	1.135	2.30	400 /	0
3	7.638	10.892	0.000	1.640	25.63	1.119	2.09	400 /	2
4	7.638	11.679	0.000	2.427	25.31	1.105	2.24	400 /	1
5	7.638	12.467	0.000	3.214	25.08	1.095	2.21	400 /	1
6	7.638	13.254	0.000	4.002	24.76	1.081	2.23	400 /	0
7	7.638	14.435	0.000	5.183	24.57	1.073	2.30	400 /	2
8	7.638	15.616	0.000	6.364	24.32	1.062	2.39	400 /	1

Table B-1m. Profile around girth, at lower edge, 29.7 knots.

Profile around girth, at lower edge.*							Tunnel speed:	29.7	knots
							Tunnel pressure:	17.0	psia
Point	X (in.)	Y (in.)	Z (in.)	Distance from surface (in.)	Velocity (knots)	Velocity (V_x/V_0)	Turbulence (%)	Number of points / outliers	
Surface	7.638	9.252	0.000	0.000					
1	7.638	9.317	0.000	0.065	26.33	0.886	9.06	400 /	0
2	7.638	10.104	0.000	0.852	33.22	1.119	1.68	400 /	1
3	7.638	10.892	0.000	1.640	32.74	1.102	1.71	400 /	2
4	7.638	11.679	0.000	2.427	32.34	1.089	1.60	400 /	0
5	7.638	12.467	0.000	3.214	31.95	1.076	1.66	400 /	0
6	7.638	13.254	0.000	4.002	31.69	1.067	1.73	400 /	0
7	7.638	14.435	0.000	5.183	31.33	1.055	1.58	400 /	1
8	7.638	15.616	0.000	6.364	31.11	1.047	1.73	400 /	0

* These profiles are graphed in Figures 11b and 18b.

Table B-1. (Continued.)

Table B-1n. Profile along upper edge, 4 inches aft of stagnation point, 29.6 knots.

Profile along upper edge, 4 inches aft of stagnation point.							Tunnel speed: 29.6 knots Tunnel pressure: 17.1 psia	
Point	X (in.)	Y (in.)	Z (in.)	Distance from surface (in.)	Velocity (knots)	Velocity (V_x/V_0)	Turbulence (%)	Number of points / outliers
Surface	3.701	-8.446	0.000					
1	3.701	-10.329	0.000	1.882	31.70	1.071	2.20	13 / 0
2	3.701	-10.919	0.000	2.473	31.40	1.061	2.09	400 / 1
3	3.701	-11.510	0.000	3.063	31.09	1.050	1.83	43 / 0
4	3.701	-12.494	0.000	4.048	30.67	1.036	1.85	400 / 0
5	3.701	-13.478	0.000	5.032	30.40	1.027	1.85	400 / 1
6	3.701	-14.463	0.000	6.016	30.24	1.022	1.85	400 / 0
7	3.701	-15.447	0.000	7.000	30.22	1.021	1.73	400 / 1

Table B-1o. Profile along upper edge, 16 inches aft of stagnation point, 22.4 knots.

Profile along upper edge, 16 inches aft of stagnation point.*							Tunnel speed: 22.4 knots Tunnel pressure: 20.0 psia	
Point	X (in.)	Y (in.)	Z (in.)	Distance from surface (in.)	Velocity (knots)	Velocity (V_x/V_0)	Turbulence (%)	Number of points / outliers
Surface	9.606	-9.478	0.000					
1	9.606	-9.541	0.000	0.063	30.21	1.349	1.79	400 / 1
2	9.606	-10.329	0.000	0.851	24.89	1.111	2.44	400 / 1
3	9.606	-11.116	0.000	1.638	24.73	1.104	2.32	400 / 0
4	9.606	-11.904	0.000	2.425	24.52	1.095	2.36	400 / 1
5	9.606	-12.691	0.000	3.213	24.34	1.087	2.20	400 / 0
6	9.606	-13.478	0.000	4.000	24.18	1.080	2.23	400 / 2
7	9.606	-14.266	0.000	4.788	24.07	1.074	2.33	400 / 0
8	9.606	-15.053	0.000	5.575	23.95	1.069	2.29	400 / 1
9	9.606	-15.841	0.000	6.362	23.88	1.066	2.30	400 / 0
10	9.606	-16.628	0.000	7.150	23.77	1.061	2.33	400 / 0

* This profile is graphed in Figures 11c and 18c.

Table B-1. (Continued.)

Table B-1p. Profile at centerline, from model to tunnel wall, 14.0 knots.

Profile at centerline, from model to tunnel wall.*								Tunnel speed:	14.0	knots
								Tunnel pressure:	20.1	psia
Point	X (in.)	Y (in.)	Z (in.)	Distance from surface (in.)	Distance from wall (in.)	Velocity (knots)	Velocity (V_x/V_0)	Turbulence (%)	Number of points / outliers	
Surface	7.638	-0.014	9.252		50.748					
1	7.638	-0.014	9.339	0.086	50.661	18.08	1.291	44.13	400 /	0
2	7.638	-0.014	10.520	1.267	49.480	15.29	1.092	3.30	400 /	2
3	7.638	-0.014	12.094	2.842	47.906	14.95	1.068	3.48	400 /	2
4	7.638	-0.014	14.063	4.811	45.937	14.66	1.047	3.58	400 /	0
5	7.638	-0.014	16.425	7.173	43.575	14.39	1.028	3.69	400 /	0
6	7.638	-0.014	22.331	13.079	37.669	14.09	1.007	3.61	400 /	1
7	7.638	-0.014	28.236	18.984	31.764	13.98	0.999	4.01	400 /	2
8	7.638	-0.014	43.197	33.945	16.803	13.91	0.993	4.05	400 /	0
9	7.638	-0.014	55.008	45.756	4.992	13.89	0.992	3.90	400 /	1
10	7.638	-0.014	58.079	48.827	1.921	13.17	0.940	5.99	400 /	0
11	7.638	-0.014	58.630	49.378	1.370	12.47	0.891	7.99	400 /	1
12	7.638	-0.014	59.417	50.165	0.583	12.50	0.893	40.91	400 /	5
13	7.638	-0.014	59.732	50.480	0.268	13.17	0.941	61.58	400 /	0
Wall	7.638	-0.014	60.000	50.748						
14	7.638	-0.014	59.024	49.771	0.976	11.95	0.853	8.50	400 /	3
15	7.638	-0.014	56.543	47.291	3.457	13.81	0.987	4.15	400 /	1
16	7.638	-0.014	49.102	39.850	10.898	13.88	0.992	4.09	400 /	1
17	7.638	-0.014	35.323	26.071	24.677	13.84	0.988	4.06	400 /	0
18	7.638	-0.014	25.087	15.834	34.913	14.04	1.003	3.89	400 /	0
19	7.638	-0.014	17.606	8.354	42.394	14.35	1.025	3.58	400 /	0
20	7.638	-0.014	15.244	5.992	44.756	14.41	1.029	3.50	400 /	1
21	7.638	-0.014	12.882	3.630	47.118	14.80	1.057	3.62	400 /	0
22	7.638	-0.014	11.307	2.055	48.693	15.10	1.079	3.47	400 /	0
23	7.638	-0.014	10.520	1.267	49.480	15.30	1.093	3.27	400 /	0
24	7.638	-0.014	9.339	0.086	50.661	18.02	1.287	51.51	45 /	0

* This profile and the similar profiles at different speeds are graphed in Figure 11a.

Table B-1. (Continued.)

Table B-1q. Profile at centerline, from model to tunnel wall, 22.8 knots.

Profile at centerline, from model to tunnel wall.*								Tunnel speed:	22.8	knots
								Tunnel pressure:	12.7	psia
Point	X (in.)	Y (in.)	Z (in.)	Distance from surface (in.)	Distance from wall (in.)	Velocity (knots)	Velocity (V_x/V_0)	Turbulence (%)	Number of points	/ outliers
Surface	7.638	-0.014	9.252		50.748					
1	7.638	-0.014	10.520	1.267	49.480	25.15	1.103	2.14	400	/ 0
2	7.638	-0.014	12.094	2.842	47.906	24.51	1.075	2.11	400	/ 2
3	7.638	-0.014	14.063	4.811	45.937	24.07	1.056	1.81	400	/ 2
4	7.638	-0.014	16.425	7.173	43.575	23.78	1.043	2.12	400	/ 1
5	7.638	-0.014	22.331	13.079	37.669	23.19	1.017	1.99	400	/ 1
6	7.638	-0.014	28.236	18.984	31.764	22.98	1.008	2.20	400	/ 1
7	7.638	-0.014	43.197	33.945	16.803	23.02	1.010	2.08	400	/ 1
8	7.638	-0.014	55.008	45.756	4.992	23.00	1.009	1.98	400	/ 0
9	7.638	-0.014	58.079	48.827	1.921	21.96	0.963	4.53	400	/ 0
10	7.638	-0.014	58.630	49.378	1.370	21.15	0.928	5.59	400	/ 0
11	7.638	-0.014	59.417	50.165	0.583	19.49	0.855	7.66	400	/ 1
12†	7.638	-0.014	59.732	50.480	0.268	19.69	0.863	21.51	400	/ 5
Wall	7.638	-0.014	60.000	50.748						
13	7.638	-0.014	59.024	49.771	0.976	20.26	0.889	7.44	400	/ 2
14	7.638	-0.014	56.543	47.291	3.457	23.14	1.015	2.29	400	/ 0
15	7.638	-0.014	49.102	39.850	10.898	23.10	1.013	2.09	400	/ 0
16	7.638	-0.014	35.323	26.071	24.677	23.17	1.016	2.12	400	/ 0
17	7.638	-0.014	25.087	15.834	34.913	23.30	1.022	2.15	400	/ 2
18	7.638	-0.014	17.606	8.354	42.394	23.72	1.041	2.06	400	/ 1
19	7.638	-0.014	15.244	5.992	44.756	24.00	1.053	1.92	400	/ 2
20	7.638	-0.014	12.882	3.630	47.118	24.47	1.073	2.01	400	/ 0
21	7.638	-0.014	11.307	2.055	48.693	25.01	1.097	2.23	400	/ 0
22	7.638	-0.014	10.520	1.267	49.480	25.34	1.112	2.23	400	/ 0

* This profile and the similar profiles at different speeds are graphed in Figure 11a. This profile is also graphed in Figure 18a.

† This point is the high turbulence data point shown in Figures 9a and 10a.

Table B-1. (Continued.)

Table B-1r. Profile at centerline, from model to tunnel wall, 29.7 knots.

Profile at centerline, from model to tunnel wall.*								Tunnel speed:	29.7	knots
								Tunnel pressure:	17.0	psia
Point	X (in.)	Y (in.)	Z (in.)	Distance from surface (in.)	Distance from wall (in.)	Velocity (knots)	Velocity (V_x/V_0)	Turbulence (%)	Number of points	/ outliers
Surface	7.638	-0.014	9.252		50.748					
1	7.638	-0.014	10.520	1.267	49.480	32.47	1.093	1.54	400	/ 2
2	7.638	-0.014	12.094	2.842	47.906	31.70	1.067	1.65	400	/ 0
3	7.638	-0.014	14.063	4.811	45.937	31.11	1.047	1.75	400	/ 1
4	7.638	-0.014	16.425	7.173	43.575	30.61	1.031	1.72	400	/ 2
5	7.638	-0.014	22.331	13.079	37.669	29.99	1.010	1.70	400	/ 1
6	7.638	-0.014	28.236	18.984	31.764	29.79	1.003	1.85	400	/ 0
7	7.638	-0.014	43.197	33.945	16.803	29.65	0.998	1.73	400	/ 1
8	7.638	-0.014	55.008	45.756	4.992	29.67	0.999	1.66	400	/ 1
9	7.638	-0.014	58.079	48.827	1.921	28.58	0.962	3.84	400	/ 1
10	7.638	-0.014	58.630	49.378	1.370	27.24	0.917	5.39	400	/ 0
11	7.638	-0.014	59.417	50.165	0.583	25.58	0.861	8.63	400	/ 5
12	7.638	-0.014	59.732	50.480	0.268	24.69	0.831	7.93	400	/ 3
Wall	7.638	-0.014	60.000	50.748						
13	7.638	-0.014	59.024	49.771	0.976	26.73	0.900	5.84	400	/ 0
14	7.638	-0.014	56.543	47.291	3.457	29.64	0.998	1.72	400	/ 0
15	7.638	-0.014	49.102	39.850	10.898	29.65	0.998	1.80	400	/ 1
16	7.638	-0.014	35.323	26.071	24.677	29.69	1.000	1.76	400	/ 0
17	7.638	-0.014	25.087	15.834	34.913	29.91	1.007	1.71	400	/ 0
18	7.638	-0.014	17.606	8.354	42.394	30.47	1.026	1.59	400	/ 0
19	7.638	-0.014	15.244	5.992	44.756	30.87	1.039	1.68	400	/ 0
20	7.638	-0.014	12.882	3.630	47.118	31.45	1.059	1.55	400	/ 2
21	7.638	-0.014	11.307	2.055	48.693	32.09	1.080	1.51	400	/ 0
22	7.638	-0.014	10.520	1.267	49.480	32.46	1.093	1.65	400	/ 2

* This profile and the similar profiles at different speeds are graphed in Figure 11a.

REFERENCES

1. Schiebe, Frank R., "Measurement of the Cavitation Susceptibility of Water Using Standard Bodies," St. Anthony Falls Hydraulic Laboratory, University of Minnesota (Feb 1972).

2. Durst, F., A. Melling, and J.H. Whitelaw, Principles and Practice of Laser-Doppler Anemometry, Academic Press, New York (1981).

3. Coleman, Hugh W. and W. Glenn Steele, Experimentation and Uncertainty Analysis for Engineers, John Wiley and Sons, New York (1989).

4. Lin, Cheng-Wen, Gerald D. Smith, and Steven C. Fisher, "Numerical Flow Simulations on the DARPA SUBOFF Configurations," DTRC/SHD-1298-09 (Jul 1990).

5. Walatka, Pamela P., Pieter G. Buning, Larry Pierce, and Patricia A. Elson, "PLOT3D User's Manual," NASA Technical Memorandum 101067 (Mar 1990).